Miner Petrol (2013) 107:679–707
DOI 10.1007/s00710-012-0210-1

SPECIAL ISSUE GONDWANA COLLISION

# Crustal age domains and metamorphic reworking of the deep crust in Northern-Central Tanzania: a U/Pb zircon and monazite age study

**V. Tenczer · Ch. Hauzenberger · H. Fritz · G. Hoinkes · S. Muhongo · U. Klötzli**

Received: 10 November 2011 / Accepted: 5 June 2012 / Published online: 20 July 2012


**Abstract** Geochronological data are presented from Northern Tanzania, where deep-crustal terranes of different age are exposed. Stacking of these terranes was diachronous with one peak around 640 Ma, defined as East African Orogeny, and final consolidation at 550–580 Ma, that is defined as Kuunga Orogeny. This later event is predominant in the Western Granulite Belt of northern Tanzania and related to thrusting onto the Tanzanian Craton. The Tanzania Craton itself experienced a polycyclic history; age domains around 2.64 Ga prevail in the studied samples. There is no evidence of the Paleoproterozoic Usagaran Belt in northern Tanzania. Here the gneisses contain relicts of reworked Archean basement and are therefore considered part of the Western Granulites. Inliers of the Western Granulites are also found in the cores of marble antiforms that are part of the upper, sedimentary sequence of the Eastern Granulites. Those inliers formed during the Kuungan orogenic phase when the Eastern Granulites have taken their final position and were folded together with the Western Granulites.

Editorial handling: M. Santosh

V. Tenczer (✉) · C. Hauzenberger · H. Fritz · G. Hoinkes
Department of Earth Sciences, University of Graz,
Graz, Austria
e-mail: tenczer@uni-graz.at

S. Muhongo
University of Dar es Salaam,
Dar es Salaam, Tanzania

U. Klötzli
Department of Lithospheric Resarch, University of Vienna,
Vienna, Austria

## Introduction

The Maasai Steppe in Northern Tanzania comprises a poorly exposed collage of different tectonic units belonging to the late Neoproterozoic to early Cambrian Mozambique Belt (Fig. 1). In addition to poor exposures, the field relationships of basement domains are obliterated by the East African Rift system seen in large faults, volcanics and volcanoclastic sediments (Hepworth 1972; Spooner 1970; Muhongo et al. 1999; Maboko 2000). Recently, this area attracted some interest by research teams with focus on lower crustal processes and reworking of Archean crust during the assembly of the supercontinent Gondwana (Fritz et al. 2009; LeGoff et al. 2010; Feneyrol et al. 2011; Blondes et al. submitted; Bellucci et al. 2011; Mansur et al. 2011). Deciphering the Precambrian history of this part of the Mozambique Belt is a complicated task due to its long-lasting, partly poly-phase tectonometamorphic history and the fact that individual crustal blocks reached high-grade metamorphism more than once in their history. Discrete tectonic features and terrane boundaries are blurred or indistinguishable in the lower crust and a geochronological study is the basis for subdivision of amalgamated terranes.

More data are available from Central Tanzania, where different tectonometamorphic units and associated large scale shear zones have been recognised (Sommer et al. 2003; Fritz et al. 2005; Cutten et al. 2006; Tenczer et al. 2007) (Fig. 1). A nappe stack of crustal units has been identified that was emplaced westwards onto the Archean Tanzania Craton. The section from western footwall to eastern hangingwall units includes: 1) The Paleoproterozoic Usagaran Belt (1.8–2.0 Ga: Möller et al. 1995; Collins et al.

2004; Sommer et al. 2005) was attached by westward thrusting onto the Tanzania Craton. 2) On top of the Usagaran Belt a Western Granulite Belt was recognised which represents a collage of poorly defined crustal pieces. Most rocks of the Western Granulites display Archean and Paleoproterozoic formation ages (Johnson et al. 2003; Cutten et al. 2006; LeGoff et al. 2010). The age of the metamorphic overprint, however, is disputed (ca. 640 Ma: Sommer et al. 2003; 530–580 Ma: Cutten et al. 2006). 3) The easternmost and uppermost sequence of the nappe pile in Tanzania is called "Eastern Granulites" with Neoproterozoic (800–1,000 Ma) juvenile formation ages and granulite facies metamorphism around 640 Ma (e.g. Möller et al. 2000). Two other units exposed in southeastern Kenya (Fig. 1) are considered as a part of the juvenile Neoproterozoic Arabian Nubian Shield (e.g., Stern 2002) and as part of the Azania micro-continent (Galana Terrane: Hauzenberger et al. 2007). The latter may represent meta-sedimentary and meta-magmatic suites emplaced and deposited at the east bank of the Mozambique Ocean (Collins and Pisarevsky 2005). Metamorphism in this unit dates around 550 Ma (Hauzenberger et al. 2007). Several west–east trending shear belts of partly unknown age modified the geometry of the orogen and probably juxtaposed different tectonic units against each other (Fritz et al. 2005; 2009).

The intention of this study is to present new geochronological data from northern Tanzania in order to unravel the tectonometamorphic history of the Maasai Steppe. One outstanding problem concerns the timing of late Neoproterozoic to Cambrian orogenic events and the potential polyphase nature of deformation and metamorphism. Ages interpreted to date peak metamorphism in the Eastern Granulites cluster around 630 Ma (e.g. Möller et al. 2000); for the Western Granulites both, 640–620 Ma ages (e.g. Sommer et al. 2003) and 550 Ma ages have been reported (e.g. Cutten et al. 2006). Hence, poly-phase deformation with complex thrust and fold geometries (Rossetti et al. 2008; Fritz et al. 2009) must be taken into account. On larger scale this problem touches the extent and delineation of the 640–620 Ma East African Orogeny and the ca. 550 Ma Kuunga Orogeny in eastern Africa (Collins and Pisarevsky 2005). Another open question addresses the distribution of distinct crustal age domains in general and the extent of the Paleoproterozoic Usagaran Belt in particular. It is unclear whether the Usagaran Belt which is exposed along the southern Tanzania Craton margin continues northwards. In northern Tanzania the Western Granulite Belt seems to be in direct contact with the Tanzania Craton (Fig. 1). This situation might be consequence of poly-phase thrusting or larger thrust displacement in the north associated with a complete overthrusting of footwall units. Here, we present geochronological data of key outcrops that shed light into the structural relationship between the different crustal blocks.

**Fig. 1** **a** Tectonic map of central—northern Tanzania and southern Kenya with the sampled spots indicated. In anticipation of the results from this study the two-phase tectonic evolution during Gondwana consolidation is shown. East African structural elements date around 630 Ma, the Kuunga event around 550 Ma. **b** Cross-sections through the orogenic belts of Tanzania (for colour code and profile location see Fig. 1a). Samples analysed in this study are projected into profile lines. Red italic numbers are published ages of peak metamorphism (Hauzenberger et al. 2007 (H); Möller et al. 2000 (M); LeGoff et al. 2010 (L); Blondes et al. submitted (B); Tenczer et al. 2006 (T)). Green italic numbers are cooling age data from Maboko 2000, 2001 (Ma)

Results will be discussed with regards to tectonic processes that finally shaped greater Gondwana.

## Geological setting

With the help of two profiles drawn through central and northern Tanzania (Fig. 1b) we shortly characterise crustal domains and summarise a succession of tectonic and metamorphic events.

The Usagaran Belt to the east of the Tanzanian Craton experienced a Paleoproterozoic orogen cycle. It is subdivided into two major litho-tectonic units, the high-grade structural basement (Isimani Suite: Mruma 1989) and the 1,920 Ma old low-grade metamorphosed volcano-sedimentary cover (Ndembera and Konse Groups: Mruma 1995; Sommer et al. 2005). The Isimani Suite contains lenticular bodies of ca. 2,000 Ma old eclogites (Möller et al. 1995; Reddy et al. 2003). Characteristic for the Usagaran are intrusions of granitoids covering ca. 50 % of the total outcrop area. Granitoids cover a time span from 1,900 Ma to 1,730 Ma (Gabert and Wendt 1974) and have been mapped as syn- to post tectonic granitoids. The Usagaran Belt was little affected by the late Neoproterozoic metmorphism. The presence of weakly deformed and metamorphosed Paleoproterozoic sediments and Paleoproterozoic K/Ar ages throughout the belt (Gabert and Wendt 1974) suggest a Neoproterozoic overprint at maximum greenschist-facies metamorphic conditions.

Hints for early Cambrian low temperature deformation and metamorphism are derived from the thrust contact to the Tanzania Craton margin. Here, Usagaran units have been thrust onto the Tanzania Craton within a thin-skinned tectonic style (Fritz et al. 2005). Discordant U/Pb rutile data derived from retrogressed Paleoproterozoic eclogite (Möller et al. 1995) fall on a reference line intersecting the Concordia at 2,010 Ma and 500 Ma. K/Ar data (Gabert and Wendt 1974) and $^{40}Ar/^{39}Ar$ data (Reddy et al. 2004) of biotite and muscovite derived from the Craton margin and Usagaran Belt range from ca. 3,200–500 Ma and support incomplete resetting during the orogeny.

The boundary between the Usagaran and Western Granulite Belt is defined, aside from lithological differences, by the first occurrence of clearly Late Neoproterozoic to

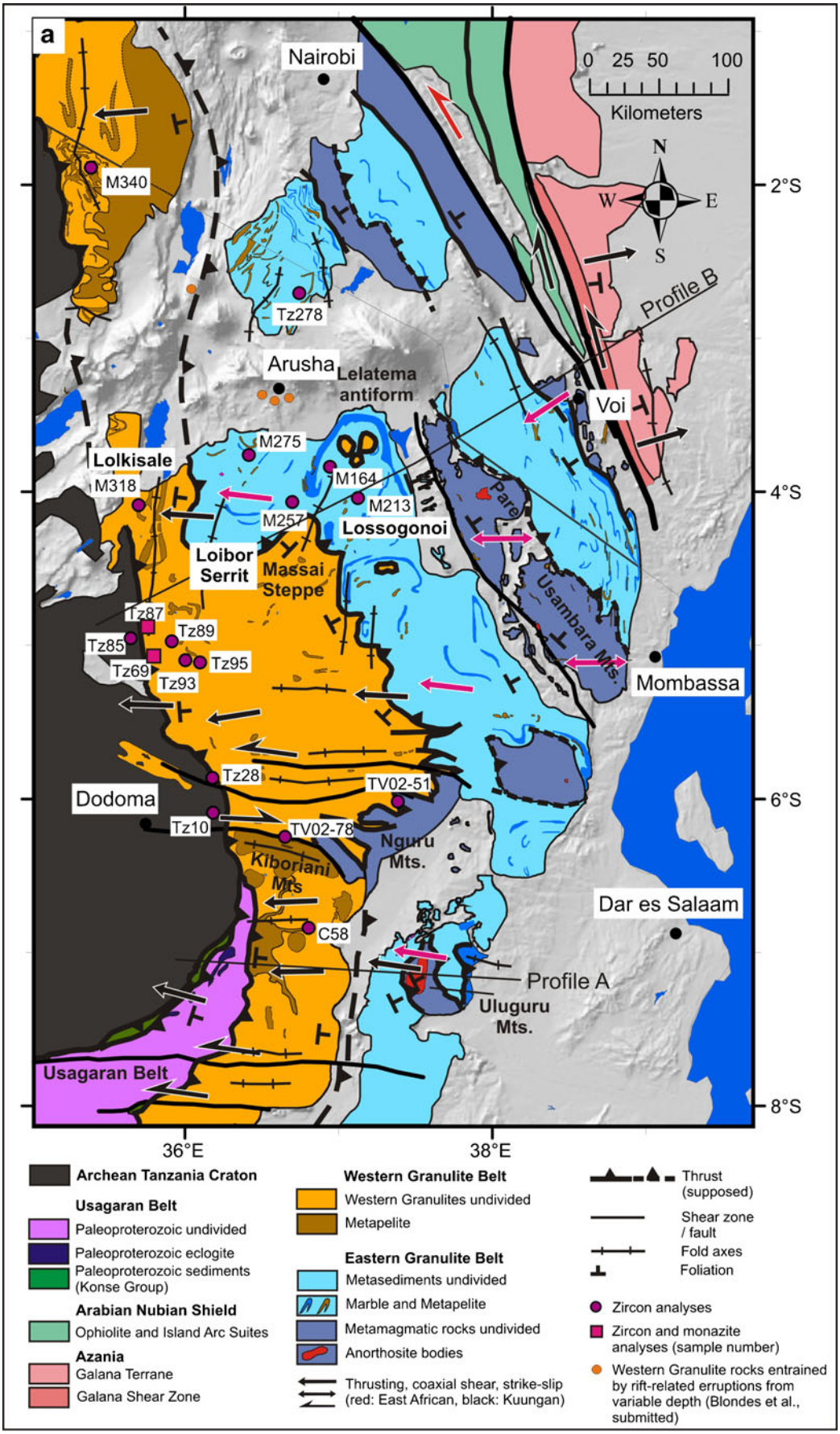
a
Nairobi
0 25 50 100
Kilometers
N
W
E
S
M340
Tz278
Arusha
Lelatema antiform
Profile B
Voi
M275
Lolkisale
M318
M164
M213
M257
Lossogonoi
Pare
Loibor Serrit
Massai Steppe
Usambara Mts.
Tz87
Tz89
Tz85
Tz95
Tz69
Tz93
Mombassa
Tz28
TV02-51
Dodoma
Tz10
TV02-78
Nguru Mts.
Kiboriani Mts
Dar es Salaam
C58
Profile A
Uluguru Mts.
Usagaran Belt
2°S
4°S
6°S
8°S
36°E
38°E
Archean Tanzania Craton
Usagaran Belt
Paleoproterozoic undivided
Paleoproterozoic eclogite
Paleoproterozoic sediments (Konse Group)
Arabian Nubian Shield
Ophiolite and Island Arc Suites
Azania
Galana Terrane
Galana Shear Zone
Western Granulite Belt
Western Granulites undivided
Metapelite
Eastern Granulite Belt
Metasediments undivided
Marble and Metapelite
Metamagmatic rocks undivided
Anorthosite bodies
Thrusting, coaxial shear, strike-slip (red: East African, black: Kuungan)
Thrust (supposed)
Shear zone / fault
Fold axes
Foliation
Zircon analyses
Zircon and monazite analyses (sample number)
Western Granulite rocks entrained by rift-related erruptions from variable depth (Blondes et al., submitted)

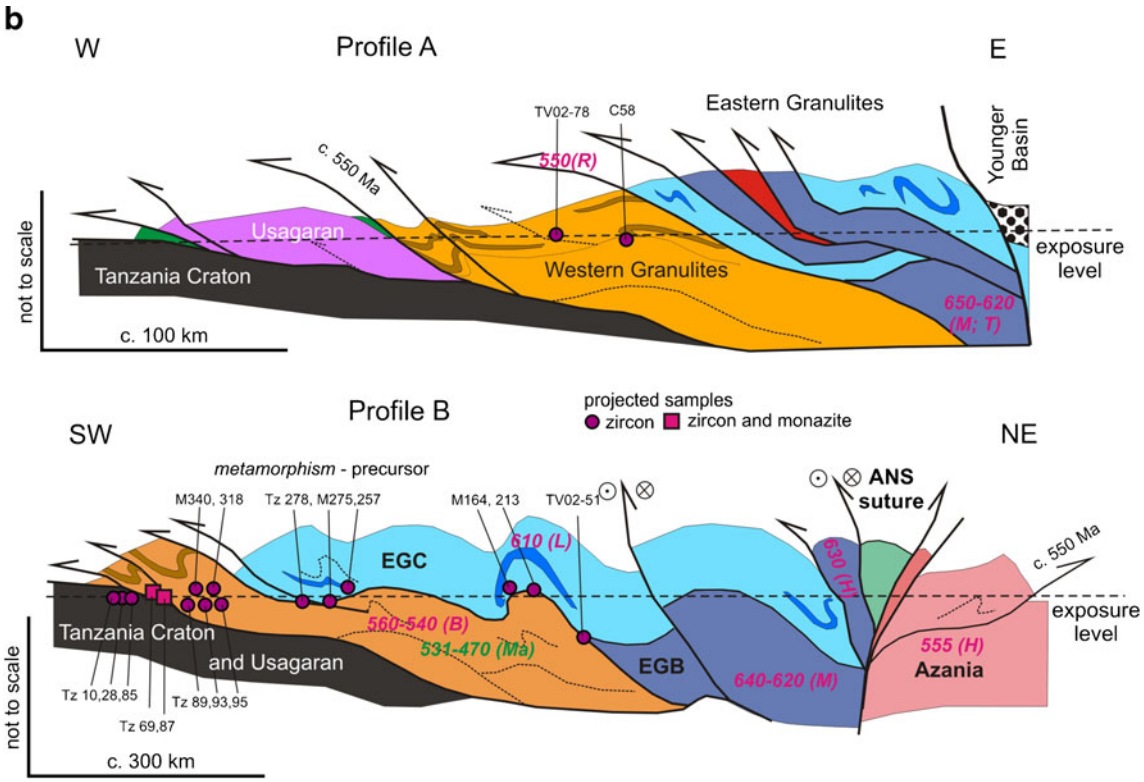


**Fig. 1** (continued)

Cambrian cooling ages (Gabert and Wendt 1974). Relative few data exist from the Western Granulite Belt; thus the nature of the crustal assembly remains speculative. Nd model ages ($T_{DM}$ Nd 2,500–3,100 Ma) from the Western Granulite Belt are indistinguishable from that of the Tanzanian Craton suggesting a predominance of reworked older crust (Maboko 1995; Möller et al. 1998). Zircon data (SHRIMP and evaporation techniques) show granitoid emplacement ages ranging from Archean (2,760 to 2,508 Ma: Johnson et al. 2003; Cutten et al. 2006), Archean-Paleoproterozoic (2,450 to 2,630 Ma: LeGoff et al. 2010) to typical Paleoproterozoic Usagaran (1,920 to 1,830 Ma: Sommer et al. 2003; Vogt et al. 2006). The rather uniform succession includes high-grade metamorphosed psammites and pelites and intercalated granitoids, amphibolites and ultramafic rocks. Meta-sedimentary rocks are concentrated in the western part of the belt (Fig. 1). Nearby Arusha Western Granulite rocks were entrained by rift related eruptions from variable depth (Blondes et al. submitted) indicating that here the Mozambique Belt is largely composed of Western Granulites and Eastern Granulites represent only a thin tectonic sheet. The contact between Western and Eastern Granulites in northern Tanzania (Fig. 1) was drawn on the basis of lithological similarities and is somewhat speculative. The course of that boundary might be revised when more data are available.

The structural style changes at the Usagaran/Western Granulites boundary from localised semi-brittle to distributed ductile fabrics showing top-to-the west displacement at elevated temperatures, i.e. upper greenschist to amphibolites facies metamorphic grade (Tenczer et al. 2007). The Western Granulites Belt experienced metamorphism and deformation up to granulite facies. However, lower grade metamorphism (amphibolite grade) is present at the western margin of the Western Granulites as inferred from muscovite bearing lithologies.

The timing and intensity of the metamorphic event (events) is strongly debated. Based on zircon rim ages some authors argue for Neo-Archean granulite facies metamorphism (2,654–2,598 Ma: Johnson et al. 2003) while from the same outcrop Sm/Nd ages of the mineral assemblage garnet and pyroxene give Neoproterozoic ages (Hauzenberger et al. 2011). For some locations Neoproterozoic metamorphism and deformation has been proposed (ca. 640 Ma: Sommer et al. 2003; Vogt et al. 2006); for other regions Late Neoproterozoic/Early Cambrian metamorphism and deformation (549–535 Ma: Cutten et al. 2006) is suggested.

Structures within the internal portions of the Western Granulites Belt display west-directed, high-vorticity, noncoaxial flow compatible with crustal thickening during emplacement onto the Tanzania Craton and the Usagaran Belt, respectively. The hangingwall boundary, i.e., contact to the Eastern Granulites is defined as ductile to semi-brittle shear

zone associated with north-westward nappe emplacement at ca. 550 Ma (Rossetti et al. 2008). This shear zone cuts the ca. 640 Ma old internal fabric within the Eastern Granulites. The superposition of structural elements gave rise to superposed folding with basin- and-dome geometry, best seen in the core of the Laletema antiform (LeGoff et al. 2010) (Fig. 1). The thrust contact between the Western and Eastern Granulites is folded around N-S to NE-SW trending fold axes (Fig. 1a,b).

The Eastern Granulites nappe complex in Tanzania has been divided into a basal unit composed largely of meta-magmatic rocks and an upper unit composed of meta-sediments including marbles (Fritz et al. 2005, 2009). The meta-magmatic suite contains anorthosite bodies as characteristic members that give overwhelmingly Neoproterozoic formation ages (900–700 Ma: for summary of ages see Tenczer et al. 2006). Sm–Nd, Rb–Sr, and Pb–Pb isotopic data (Möller et al. 1998; Maboko et al. 1985, 1989) suggest that most magmatic rocks formed during the Neoproterozoic as also evidenced from εNd—model ages of about 1,000 Ma. Based on this fact, Maboko and Nakamura (2002) inferred that the Eastern Granulites represent Neoproterozoic juvenile crust that formed coeval with that of the Arabian Nubian Shield. We emphasise, however, that not all rocks of the Eastern Granulites display juvenile Neoproterozoic isotopic signatures. Different anorthosites and gneisses from the Eastern Granulites contain Archean and Paleoproterozoic, but no Mesoproterozoic zircon (Tenczer et al. 2006; LeGoff et al. 2010). The meta-sediments contain ruby bearing marbles as distinctive lithology (Fritz et al. 2009; LeGoff et al. 2010; Feneyrol et al. 2011). Depositional ages of comparable marbles exposed in the Cabo Delgado Nappe Complex of Mozambique have been narrowed down by $^{87}Sr/^{86}Sr$ isotopic studies (Melezhik et al. 2008). Except one estimate of 1,250–910 Ma, all other data point to Neoproterozoic deposition of limestone protoliths between 800 and 660 Ma.

High pressure Granulite facies metamorphism of the Eastern Granulites was dated between 655 and 600 Ma (Appel et al. 1998; Hauzenberger et al. 2004; Möller et al. 2000; Tenczer et al. 2011). Tectonic styles and the pressure temperature evolutionary path from the meta-magmatic basement display subhorizontal high temperature flow at partly extreme temperature conditions (exceeding 900 °C at peak pressures between 1.2 and 1.4 GPa). Top-to-the west tectonic transport is occasionally recorded, however, melt assistant coaxial flow is dominant (Fritz et al. 2005, 2009). By contrast to the horizontal, coaxial W-E stretch within the meta-magmatic basement, the meta-sedimentary cover suites experienced W-E to NW-SE horizontal shortening, as best evidenced from upright, N-S trending folds in distinct marble beds (Fig. 1).

The southern limit of the Arabian Nubian Shield, defined as Voi Suture (Frisch and Pohl 1986) comprises Neoproterozoic island arc suites that are exposed in southern Kenya (Fig. 1). The Galana Terrane to the east of it is considered as a part of Azania and experienced east-directed stacking and folding of continental units together with granulite facies metamorphism (peak P-T 800 °C/0.9 GPa) at 580–540 Ma (Hauzenberger et al. 2004, 2007).

## Methodoloy

A set of 15 samples has been selected for this geochronological investigation. Most of them are derived from supposed Western Granulites, the least studied unit in Tanzania. Sample locations are shown in Fig. 1 and projected into a W-E profile constructed for northern Tanzania (Fig. 1b). Samples TZ10, TZ28 and TZ85 are derived from the Tanzania Craton close to the Western Granulites boundary. Samples TZ 69, TZ 87, M 340, M318, TZ 89, TZ93 and TZ95 are intended as W-E profile through Western Granulites with the majority of sampling points close to the Tanzania Craton. TZ278, M275, M257, M164 and M213 are taken from the area mapped as Eastern Granulites, close to the boundary to Western Granulites. However, numerous antiforms with rocks from the Western Granulites occur as domes within the Eastern Granulites (Fritz et al. 2009; LeGoff et al. 2010). Not all of them are properly mapped. Hence, some of these samples are taken to shed light on the existence of Western Granulites windows within the Eastern Granulites. All samples fulfil the criteria that they are rich in the accessory minerals zircon/monazite, have promising internal textures and stem from key outcrops of crucial positions in the orogen (Figs. 2, 3 and 4).

Most of the samples have been analysed using the LA-ICP-MS method. Only the samples TV02-78, TV02-51 and C58 (Fig. 5) have been investigated in another measuring campaign with SIMS for its isotopic ratios. For the detailed analytical procedure see the Appendix. The analyses are presented in Table 1 for the LA-ICP-MS data and in Table 2 for the SIMS data. Mineral abbreviations are followed the suggestions of Kretz (1983).

## Sample description and analytical results: the Tanzania Craton boundary

The Tanzania Craton of central Tanzania is overthrusted by the Paleoproterozoic Usagaran Belt that is narrowing to the north (Fig. 1) (Fritz et al. 2005 and references therein). Both units, the Craton and the Usagaran Belt are dominated by magmatic rocks of granitic to tonalitic composition. A distinction between both units is mainly possible by an age determination of igneous rocks. The protolith ages of the

**Table 1** U-Pb analytical results from measuring campaigns using the LA-MC-ICP-MS technique (in Vienna and Bergen). Isotopic results from LA-ICPMS and calculated ages

| | Final blank corrected intensities (in V) | | | | Final mass bias corrected ratios | | | | | | | Calculated ages | | | | | |
|---|---|---|---|---|---|---|---|---|---|---|---|---|---|---|---|---|---|
| | $^{204}Pb$ | $^{206}Pb$ | $^{207}Pb$ | $^{238}U$ | $^{207}Pb/^{235}U$ | 2σ | $^{206}Pb/^{238}U$ | 2σ | Rho | $^{207}Pb/^{206}Pb$ | 2σ | $^{207}Pb/^{235}U$ | 2σ | $^{206}Pb/^{238}U$ | 2σ | $^{207}Pb/^{206}Pb$ | 2σ |
| TZ10 | | | | | | | | | | | | | | | | | |
| _23_1 | 1.50E-04 | 9.53E–03 | 1.07E–03 | 8.30E–03 | 8.4759 | 0.6986 | 0.2693 | 0.0336 | 0.7564 | 0.2235 | 0.0405 | 2283 | 75 | 1537 | 171 | 3006 | 295 |
| _25_1jung | 2.84E–04 | 1.10E–02 | 1.52E–03 | 1.56E–02 | 6.5290 | 1.3253 | 0.1864 | 0.0465 | 0.5621 | 0.2515 | 0.0143 | 2050 | 181 | 1102 | 253 | 3194 | 90 |
| _25_2 | 8.73E–05 | 6.09E–03 | 6.76E–04 | 7.70E–03 | 5.6237 | 1.0977 | 0.1789 | 0.0445 | 0.6374 | 0.2228 | 0.0114 | 1920 | 170 | 1061 | 243 | 3001 | 82 |
| _34_1neu | 7.08E–05 | 8.95E–03 | 9.46E–04 | 6.17E–03 | 10.9264 | 1.4263 | 0.3508 | 0.0475 | 0.4811 | 0.2205 | 0.0045 | 2517 | 122 | 1938 | 227 | 2984 | 33 |
| _15_1 | 5.85E–05 | 1.90E–02 | 1.93E–03 | 1.21E–02 | 10.8853 | 2.0613 | 0.3700 | 0.0748 | 0.5336 | 0.2057 | 0.0052 | 2513 | 178 | 2030 | 352 | 2872 | 41 |
| _19_1 | 3.85E–05 | 1.02E–02 | 9.55E–04 | 6.71E–03 | 9.6711 | 0.8636 | 0.3786 | 0.0292 | 0.4321 | 0.1821 | 0.0132 | 2404 | 82 | 2070 | 137 | 2672 | 121 |
| _19_2neu | 7.58E–06 | 2.41E–03 | 1.68E–04 | 2.49E–03 | 5.6567 | 0.7087 | 0.3086 | 0.0310 | 0.4011 | 0.1400 | 0.0078 | 1925 | 109 | 1734 | 153 | 2227 | 97 |
| TZ28 | | | | | | | | | | | | | | | | | |
| _6_1 | 2.66E–05 | 1.87E–02 | 2.35E–03 | 1.28E–02 | 12.0355 | 0.4240 | 0.4676 | 0.0171 | 0.5198 | 0.1869 | 0.0018 | 2607 | 33 | 2473 | 75 | 2715 | 16 |
| _2_1 | 3.29E–06 | 1.44E–03 | 1.58E–04 | 8.91E–04 | 12.2726 | 0.7976 | 0.5530 | 0.0348 | 0.4837 | 0.1614 | 0.0015 | 2625 | 61 | 2838 | 144 | 2470 | 16 |
| _2_2 | 4.67E–05 | 4.73E–03 | 6.59E–04 | 3.30E–03 | 13.6543 | 0.6830 | 0.4661 | 0.0276 | 0.5920 | 0.2112 | 0.0034 | 2726 | 47 | 2466 | 121 | 2915 | 26 |
| _7_1 | 4.39E–06 | 3.43E–03 | 4.25E–04 | 2.12E–03 | 13.3987 | 0.3169 | 0.5428 | 0.0111 | 0.4312 | 0.1798 | 0.0017 | 2708 | 22 | 2795 | 46 | 2651 | 15 |
| _8_1 | 4.87E–06 | 4.22E–03 | 4.88E–04 | 2.70E–03 | 12.0504 | 0.1394 | 0.5099 | 0.0065 | 0.5480 | 0.1707 | 0.0005 | 2608 | 11 | 2656 | 28 | 2564 | 5 |
| _29_1 | 2.12E–06 | 2.00E–03 | 2.39E–04 | 1.32E–03 | 12.2518 | 0.5797 | 0.5309 | 0.0162 | 0.3221 | 0.1697 | 0.0037 | 2624 | 44 | 2745 | 68 | 2555 | 36 |
| _29_2 | 1.22E–05 | 3.06E–03 | 3.87E–04 | 2.19E–03 | 12.3547 | 0.5269 | 0.5106 | 0.0219 | 0.5032 | 0.1757 | 0.0018 | 2632 | 40 | 2659 | 94 | 2613 | 17 |
| _35_1 | 1.10E–05 | 1.53E–02 | 1.83E–03 | 1.01E–02 | 12.2888 | 0.4280 | 0.5161 | 0.0175 | 0.4861 | 0.1723 | 0.0006 | 2627 | 33 | 2683 | 74 | 2580 | 6 |
| _40_1 | 8.93E–06 | 1.35E–02 | 1.63E–03 | 8.86E–03 | 12.5725 | 0.1729 | 0.5280 | 0.0076 | 0.5227 | 0.1730 | 0.0009 | 2648 | 13 | 2733 | 32 | 2587 | 8 |
| TZ85 | | | | | | | | | | | | | | | | | |
| _5_1 | 4.67E–06 | 7.16E–03 | 8.63E–04 | 4.82E–03 | 12.1892 | 0.9805 | 0.5308 | 0.0430 | 0.5034 | 0.1661 | 0.0013 | 2619 | 76 | 2745 | 181 | 2519 | 14 |
| _5_2 | 9.60E–06 | 4.44E–03 | 4.95E–04 | 5.40E–03 | 6.1466 | 1.1160 | 0.2746 | 0.0421 | 0.4219 | 0.1582 | 0.0017 | 1997 | 160 | 1564 | 213 | 2436 | 18 |
| _7_1 | 1.58E–04 | 2.13E–02 | 3.09E–03 | 2.35E–02 | 8.8563 | 0.9476 | 0.3239 | 0.0242 | 0.3488 | 0.1933 | 0.0083 | 2323 | 98 | 1809 | 118 | 2770 | 71 |
| _9_1 | 1.76E–04 | 1.54E–02 | 2.17E–03 | 2.72E–02 | 4.8736 | 0.6548 | 0.1778 | 0.0253 | 0.5296 | 0.2042 | 0.0025 | 1798 | 114 | 1055 | 139 | 2860 | 20 |
| _11_1 | 4.33E–05 | 1.18E–02 | 1.52E–03 | 1.17E–02 | 8.4008 | 1.4974 | 0.3313 | 0.0595 | 0.5041 | 0.1841 | 0.0016 | 2275 | 163 | 1845 | 288 | 2690 | 14 |
| _11_2 | 4.90E–05 | 8.94E–03 | 1.12E–03 | 9.53E–03 | 8.0585 | 1.0712 | 0.3288 | 0.0449 | 0.5134 | 0.1781 | 0.0017 | 2238 | 121 | 1833 | 218 | 2635 | 15 |
| _12_1 | 6.41E–05 | 7.68E–03 | 1.02E–03 | 8.55E–03 | 7.7984 | 1.9719 | 0.2871 | 0.0803 | 0.5529 | 0.1985 | 0.0040 | 2208 | 232 | 1627 | 403 | 2814 | 33 |
| TZ69 | | | | | | | | | | | | | | | | | |
| _2_1 | 5.62E–06 | 2.62E–03 | 3.12E–04 | 1.68E–03 | 13.0271 | 1.5313 | 0.5544 | 0.0636 | 0.4875 | 0.1704 | 0.0021 | 2682 | 111 | 2844 | 264 | 2561 | 20 |
| _7_1 | 5.61E–06 | 7.03E–03 | 8.86E–04 | 4.72E–03 | 12.5463 | 0.5174 | 0.5130 | 0.0220 | 0.5203 | 0.1780 | 0.0024 | 2646 | 39 | 2669 | 94 | 2634 | 22 |
| _17_1 | 5.92E–06 | 1.10E–02 | 1.38E–03 | 8.36E–03 | 11.3693 | 0.4578 | 0.4746 | 0.0216 | 0.5656 | 0.1718 | 0.0059 | 2554 | 38 | 2504 | 95 | 2575 | 57 |
| _23_1 | 4.46E–06 | 3.53E–03 | 4.39E–04 | 2.57E–03 | 11.6964 | 0.8778 | 0.4895 | 0.0362 | 0.4929 | 0.1738 | 0.0023 | 2580 | 70 | 2568 | 157 | 2594 | 22 |
| _40_1 | 5.30E–06 | 5.30E–03 | 7.12E–04 | 4.01E–03 | 12.3313 | 0.5150 | 0.4860 | 0.0205 | 0.5058 | 0.1849 | 0.0021 | 2630 | 39 | 2554 | 89 | 2697 | 19 |
| TZ87 | | | | | | | | | | | | | | | | | |
| _03_1 | 9.31E–06 | 1.72E–02 | 2.19E–03 | 1.22E–02 | 12.8933 | 1.4778 | 0.5033 | 0.0564 | 0.4887 | 0.1849 | 0.0018 | 2672 | 108 | 2628 | 242 | 2697 | 16 |
| _03_2 | 6.95E–06 | 1.23E–02 | 1.56E–03 | 8.59E–03 | 12.6164 | 0.5949 | 0.5033 | 0.0195 | 0.4107 | 0.1818 | 0.0026 | 2651 | 44 | 2628 | 84 | 2669 | 23 |
| _07_1 | 1.89E–05 | 2.45E–04 | 5.32E–05 | 5.42E–04 | 7.1259 | 0.2943 | 0.1583 | 0.0056 | 0.4300 | 0.3292 | 0.0094 | 2127 | 37 | 947 | 31 | 3613 | 44 |
| _23_1 | 1.39E–04 | 6.48E–03 | 1.20E–03 | 6.68E–03 | 12.9597 | 1.0470 | 0.3320 | 0.0294 | 0.5485 | 0.2819 | 0.0061 | 2677 | 76 | 1848 | 142 | 3373 | 34 |
| _36_1 | 1.22E–04 | 7.69E–03 | 1.34E–03 | 8.51E–03 | 11.5887 | 0.7119 | 0.3179 | 0.0231 | 0.5922 | 0.2713 | 0.0081 | 2572 | 57 | 1779 | 113 | 3314 | 47 |
| _39_1 | 3.53E–04 | 5.59E–03 | 1.56E–03 | 8.95E–03 | 12.4927 | 0.4619 | 0.1681 | 0.0156 | 0.5000 | 0.4845 | 0.0134 | 2642 | 35 | 1001 | 86 | 4195 | 41 |
| _42_1 | 1.32E–04 | 3.58E–03 | 7.74E–04 | 4.75E–03 | 12.6760 | 0.6746 | 0.2707 | 0.0195 | 0.6773 | 0.3574 | 0.0102 | 2656 | 50 | 1544 | 99 | 3739 | 43 |

**Table 1** (continued)

| | Final blank corrected intensities (in V) | | | | Final mass bias corrected ratios | | | | | | | Calculated ages | | | | | |
|---|---|---|---|---|---|---|---|---|---|---|---|---|---|---|---|---|---|
| | $^{204}Pb$ | $^{206}Pb$ | $^{207}Pb$ | $^{238}U$ | $^{207}Pb/^{235}U$ | 2σ | $^{206}Pb/^{238}U$ | 2σ | Rho | $^{207}Pb/^{206}Pb$ | 2σ | $^{207}Pb/^{235}U$ | 2σ | $^{206}Pb/^{238}U$ | 2σ | $^{207}Pb/^{206}Pb$ | 2σ |
| TZ89 | | | | | | | | | | | | | | | | | |
| _3_1 | 8.55E–06 | 1.51E–02 | 1.79E–03 | 7.88E–03 | 11.2397 | 0.5249 | 0.4422 | 0.0197 | 0.4775 | 0.1804 | 0.0007 | 2543 | 44 | 2360 | 88 | 2656 | 6 |
| _19_1 | 5.11E–06 | 7.54E–03 | 8.84E–04 | 4.69E–03 | 10.5976 | 0.2415 | 0.4304 | 0.0097 | 0.4959 | 0.1771 | 0.0007 | 2489 | 21 | 2308 | 44 | 2626 | 7 |
| _24_1 | 4.31E–06 | 7.75E–03 | 9.56E–04 | 4.79E–03 | 10.7684 | 0.5706 | 0.4149 | 0.0196 | 0.4451 | 0.1866 | 0.0018 | 2503 | 49 | 2237 | 89 | 2713 | 16 |
| _33_1 | 5.39E–06 | 6.23E–03 | 7.57E–04 | 4.34E–03 | 11.0530 | 0.6435 | 0.4504 | 0.0199 | 0.3800 | 0.1805 | 0.0020 | 2528 | 54 | 2397 | 89 | 2658 | 18 |
| _33_2 | 3.66E–06 | 6.68E–03 | 8.07E–04 | 4.89E–03 | 10.4072 | 0.4435 | 0.4275 | 0.0152 | 0.4170 | 0.1794 | 0.0011 | 2472 | 39 | 2294 | 69 | 2648 | 10 |
| _33_3 | 5.04E–06 | 3.28E–03 | 4.04E–04 | 2.30E–03 | 12.0099 | 1.0255 | 0.4743 | 0.0402 | 0.4961 | 0.1846 | 0.0018 | 2605 | 80 | 2503 | 176 | 2694 | 16 |
| _38_1 | 8.06E–06 | 9.18E–03 | 1.07E–03 | 6.38E–03 | 11.7082 | 0.3408 | 0.4626 | 0.0113 | 0.4185 | 0.1848 | 0.0072 | 2581 | 27 | 2451 | 50 | 2697 | 65 |
| _38_2 | 5.03E–06 | 8.19E–03 | 9.55E–04 | 5.77E–03 | 11.2705 | 0.5993 | 0.4744 | 0.0246 | 0.4873 | 0.1726 | 0.0006 | 2546 | 50 | 2503 | 107 | 2583 | 6 |
| TZ95 | | | | | | | | | | | | | | | | | |
| _42_1 (rim) | 4.46E–06 | 2.59E–03 | 2.53E–04 | 1.37E–03 | 10.3658 | 1.1207 | 0.4316 | 0.0458 | 0.4911 | 0.1778 | 0.0034 | 2468 | 100 | 2313 | 206 | 2632 | 32 |
| _42_2 (core) | 2.18E–05 | 2.00E–02 | 2.17E–03 | 1.10E–02 | 9.9749 | 0.5306 | 0.3894 | 0.0132 | 0.3184 | 0.1876 | 0.0033 | 2432 | 49 | 2120 | 61 | 2721 | 29 |
| _30_1 (core) | 1.56E–05 | 1.59E–02 | 1.70E–03 | 8.56E–03 | 10.5872 | 0.2580 | 0.4113 | 0.0100 | 0.4964 | 0.1874 | 0.0008 | 2488 | 23 | 2221 | 45 | 2720 | 7 |
| _30_2 (rim) | 7.12E–06 | 2.57E–03 | 2.55E–04 | 1.33E–03 | 10.4229 | 0.6786 | 0.4382 | 0.0294 | 0.5152 | 0.1720 | 0.0017 | 2473 | 60 | 2342 | 132 | 2577 | 17 |
| _19_1 | 8.46E–06 | 8.52E–03 | 8.85E–04 | 4.14E–03 | 11.3921 | 0.3214 | 0.4797 | 0.0132 | 0.4891 | 0.1729 | 0.0008 | 2556 | 26 | 2526 | 58 | 2586 | 8 |
| _20_1 | 1.57E–05 | 1.60E–02 | 1.71E–03 | 7.01E–03 | 13.0102 | 0.4872 | 0.5206 | 0.0201 | 0.5166 | 0.1775 | 0.0040 | 2680 | 35 | 2702 | 85 | 2630 | 37 |
| _14_1 | 1.41E–05 | 9.58E–03 | 1.09E–03 | 5.41E–03 | 10.5160 | 0.2091 | 0.3950 | 0.0076 | 0.4870 | 0.1928 | 0.0007 | 2481 | 18 | 2146 | 35 | 2767 | 6 |
| _15_1 | 1.64E–05 | 1.18E–02 | 1.31E–03 | 7.50E–03 | 8.9813 | 0.1336 | 0.3460 | 0.0049 | 0.4784 | 0.1849 | 0.0006 | 2336 | 14 | 1915 | 24 | 2697 | 5 |
| _13_1 | 2.03E–05 | 2.34E–02 | 2.86E–03 | 1.38E–02 | 10.7209 | 0.2681 | 0.3793 | 0.0103 | 0.5454 | 0.2048 | 0.0019 | 2499 | 23 | 2073 | 48 | 2865 | 15 |
| _14_2 | 2.60E–05 | 9.56E–03 | 1.05E–03 | 9.60E–03 | 5.2528 | 0.3572 | 0.2120 | 0.0139 | 0.4811 | 0.1808 | 0.0009 | 1861 | 58 | 1240 | 74 | 2661 | 9 |
| _08_1 | 0.00E+00 | 1.01E–02 | 1.03E–03 | 7.76E–03 | 8.1111 | 0.5654 | 0.3637 | 0.0281 | 0.5541 | 0.1205 | 0.0077 | 2243 | 63 | 2000 | 133 | 1963 | 115 |
| _03_1 | 1.78E–05 | 1.84E–02 | 2.14E–03 | 9.72E–03 | 11.0663 | 0.3295 | 0.4391 | 0.0120 | 0.4596 | 0.1854 | 0.0013 | 2529 | 28 | 2347 | 54 | 2702 | 11 |
| TZ93 | | | | | | | | | | | | | | | | | |
| _12_1 | 4.39E–06 | 7.49E–03 | 8.04E–04 | 3.76E–03 | 10.5284 | 0.6829 | 0.4571 | 0.0252 | 0.4257 | 0.1681 | 0.0013 | 2482 | 60 | 2427 | 112 | 2539 | 13 |
| _15_1 | 8.80E–06 | 7.31E–03 | 8.25E–04 | 4.25E–03 | 10.7003 | 0.3633 | 0.4381 | 0.0144 | 0.4856 | 0.1752 | 0.0008 | 2497 | 32 | 2342 | 65 | 2608 | 8 |
| _20_1 | 3.63E–06 | 1.97E–03 | 2.53E–04 | 1.05E–03 | 13.1495 | 0.4790 | 0.4716 | 0.0176 | 0.5119 | 0.1988 | 0.0014 | 2690 | 34 | 2490 | 77 | 2816 | 11 |
| _26_1 | 9.91E–05 | 9.41E–03 | 1.34E–03 | 4.33E–02 | 1.0986 | 0.5183 | 0.0371 | 0.0163 | 0.4659 | 0.2139 | 0.0083 | 753 | 256 | 235 | 101 | 2935 | 63 |
| _44_1 | 6.16E–06 | 6.42E–03 | 8.31E–04 | 2.91E–03 | 14.1284 | 0.6629 | 0.5111 | 0.0232 | 0.4840 | 0.1989 | 0.0007 | 2758 | 45 | 2661 | 99 | 2817 | 6 |
| _39_1 | 2.31E–05 | 6.60E–03 | 8.41E–04 | 7.20E–03 | 7.1769 | 0.4458 | 0.2579 | 0.0165 | 0.5154 | 0.1965 | 0.0018 | 2134 | 55 | 1479 | 85 | 2798 | 15 |
| M318 | | | | | | | | | | | | | | | | | |
| _2_2 | 4.43E–06 | 2.92E–03 | 5.31E–04 | 2.65E–03 | 11.2565 | 0.4088 | 0.4459 | 0.0135 | 0.4165 | 0.1824 | 0.0022 | 2545 | 34 | 2377 | 60 | 2675 | 20 |
| _3_1 | 1.64E–05 | 1.84E–02 | 3.48E–03 | 1.82E–02 | 12.3386 | 0.8718 | 0.4652 | 0.0305 | 0.4646 | 0.1926 | 0.0020 | 2631 | 66 | 2462 | 134 | 2765 | 17 |
| _10_1 | 3.95E–06 | 8.87E–04 | 1.56E–04 | 1.52E–03 | 5.5913 | 1.1627 | 0.2278 | 0.0506 | 0.5341 | 0.1777 | 0.0027 | 1915 | 181 | 1323 | 266 | 2631 | 25 |
| _10_2 | 8.86E–06 | 1.41E–02 | 2.62E–03 | 1.29E–02 | 11.3368 | 0.4631 | 0.4415 | 0.0175 | 0.4865 | 0.1868 | 0.0010 | 2551 | 38 | 2357 | 78 | 2714 | 8 |
| _16_1 | 1.19E–05 | 1.39E–02 | 2.57E–03 | 1.35E–02 | 10.5191 | 0.6032 | 0.4238 | 0.0186 | 0.3831 | 0.1814 | 0.0019 | 2482 | 53 | 2278 | 84 | 2666 | 17 |
| _16_2 | 5.40E–06 | 2.78E–03 | 4.09E–04 | 5.18E–03 | 5.5111 | 0.7448 | 0.2627 | 0.0263 | 0.3705 | 0.1529 | 0.0074 | 1902 | 117 | 1504 | 134 | 2378 | 83 |
| _9_1 | 7.63E–06 | 2.19E–03 | 2.33E–04 | 1.01E–02 | 1.2531 | 0.1997 | 0.0887 | 0.0082 | 0.2915 | 0.1008 | 0.0095 | 825 | 90 | 548 | 49 | 1638 | 175 |
| M340 | | | | | | | | | | | | | | | | | |
| _1_1 | 1.95E–06 | 2.17E–03 | 1.54E–04 | 5.52E–03 | 1.5900 | 0.0563 | 0.1541 | 0.0054 | 0.4939 | 0.0744 | 0.0010 | 966 | 22 | 924 | 30 | 1053 | 27 |
| _4_1 | 6.82E–06 | 1.29E–03 | 8.78E–05 | 8.44E–03 | 0.6259 | 0.0791 | 0.0667 | 0.0084 | 0.4990 | 0.0769 | 0.0041 | 494 | 49 | 416 | 51 | 1119 | 106 |
| _4_2 | 3.67E–06 | 9.64E–04 | 6.56E–05 | 2.42E–03 | 1.5406 | 0.0714 | 0.1599 | 0.0044 | 0.2952 | 0.0702 | 0.0020 | 947 | 29 | 956 | 24 | 934 | 59 |

**Table 1** (continued)

| | Final blank corrected intensities (in V) | | | | Final mass bias corrected ratios | | | | | | | Calculated ages | | | | | |
|---|---|---|---|---|---|---|---|---|---|---|---|---|---|---|---|---|---|
| | $^{204}$Pb | $^{206}$Pb | $^{207}$Pb | $^{238}$U | $^{207}$Pb/$^{235}$U | 2σ | $^{206}$Pb/$^{238}$U | 2σ | Rho | $^{207}$Pb/$^{206}$Pb | 2σ | $^{207}$Pb/$^{235}$U | 2σ | $^{206}$Pb/$^{238}$U | 2σ | $^{207}$Pb/$^{206}$Pb | 2σ |
| _12_1 | 3.95E–06 | 7.51E–04 | 5.32E–05 | 2.03E–03 | 1.4971 | 0.1265 | 0.1479 | 0.0104 | 0.4172 | 0.0737 | 0.0026 | 929 | 51 | 889 | 59 | 1034 | 72 |
| _10_1 | 4.54E–06 | 1.77E–03 | 1.22E–04 | 6.74E–03 | 0.9914 | 0.1670 | 0.0975 | 0.0172 | 0.5223 | 0.0727 | 0.0029 | 699 | 85 | 600 | 101 | 1005 | 80 |
| _15_1 | 2.18E–06 | 6.90E–04 | 4.81E–05 | 1.77E–03 | 1.5428 | 0.1085 | 0.1524 | 0.0100 | 0.4681 | 0.0717 | 0.0025 | 948 | 43 | 914 | 56 | 978 | 70 |
| _15_2 | 3.75E–06 | 1.96E–03 | 1.30E–04 | 1.06E–02 | 0.6160 | 0.1045 | 0.0628 | 0.0141 | 0.6619 | 0.0710 | 0.0033 | 487 | 66 | 393 | 86 | 956 | 94 |
| TZ278 | | | | | | | | | | | | | | | | | |
| _11_1 | 4.08E–06 | 1.21E–03 | 1.17E–04 | 4.25E–04 | 10.5868 | 0.8888 | 0.4288 | 0.0399 | 0.5536 | 0.1752 | 0.0048 | 2488 | 78 | 2300 | 180 | 2608 | 46 |
| _17_1 | 9.45E–06 | 1.33E–02 | 1.33E–03 | 4.78E–03 | 10.0995 | 0.2546 | 0.4201 | 0.0073 | 0.3437 | 0.1675 | 0.0029 | 2444 | 23 | 2261 | 33 | 2533 | 29 |
| _25_1 | 4.96E–06 | 2.65E–03 | 2.48E–04 | 9.85E–04 | 9.6750 | 0.2126 | 0.4110 | 0.0086 | 0.4771 | 0.1646 | 0.0014 | 2404 | 20 | 2219 | 39 | 2503 | 15 |
| _24_1 | 7.70E–06 | 8.75E–03 | 8.30E–04 | 2.94E–03 | 10.6848 | 0.2366 | 0.4443 | 0.0090 | 0.4560 | 0.1692 | 0.0010 | 2496 | 21 | 2370 | 40 | 2549 | 10 |
| _31_1 | 5.53E–06 | 7.49E–03 | 7.53E–04 | 3.34E–03 | 10.5312 | 0.2501 | 0.4226 | 0.0104 | 0.5196 | 0.1805 | 0.0013 | 2483 | 22 | 2272 | 47 | 2657 | 12 |
| _33_1 | 2.82E–06 | 4.09E–03 | 3.72E–04 | 1.67E–03 | 10.3200 | 0.2026 | 0.4483 | 0.0084 | 0.4766 | 0.1654 | 0.0014 | 2464 | 18 | 2388 | 37 | 2512 | 14 |
| _33_2 | 7.60E–06 | 7.12E–03 | 7.16E–04 | 3.03E–03 | 11.2523 | 0.2590 | 0.4343 | 0.0100 | 0.5010 | 0.1838 | 0.0006 | 2544 | 21 | 2325 | 45 | 2688 | 6 |
| M275 | | | | | | | | | | | | | | | | | |
| _1_1 | 4.05E–06 | 1.20E–03 | 2.01E–04 | 1.21E–03 | 9.2744 | 0.6846 | 0.4114 | 0.0261 | 0.4305 | 0.1639 | 0.0027 | 2365 | 68 | 2221 | 119 | 2497 | 28 |
| _6_1 | 1.52E–05 | 6.62E–03 | 1.09E–03 | 1.73E–02 | 7.1338 | 0.8393 | 0.3206 | 0.0369 | 0.4890 | 0.1630 | 0.0013 | 2128 | 105 | 1793 | 180 | 2487 | 14 |
| _6_2 | 4.05E–06 | 1.53E–03 | 2.51E–04 | 2.03E–03 | 7.2137 | 0.4927 | 0.3247 | 0.0213 | 0.4810 | 0.1621 | 0.0018 | 2138 | 61 | 1813 | 104 | 2478 | 19 |
| _29_1 | 2.94E–06 | 3.87E–03 | 6.58E–04 | 4.10E–03 | 7.1021 | 0.5403 | 0.3348 | 0.0190 | 0.3734 | 0.1513 | 0.0043 | 2124 | 68 | 1862 | 92 | 2361 | 49 |
| _29_2 | 4.40E–06 | 8.40E–03 | 1.34E–03 | 1.02E–02 | 8.6435 | 0.9291 | 0.3946 | 0.0352 | 0.4150 | 0.1633 | 0.0077 | 2301 | 98 | 2144 | 163 | 2490 | 80 |
| _30_1 | 6.47E–06 | 9.01E–03 | 1.55E–03 | 8.42E–03 | 10.8297 | 0.1029 | 0.4665 | 0.0047 | 0.5350 | 0.1679 | 0.0005 | 2509 | 9 | 2468 | 21 | 2536 | 5 |
| M257 | | | | | | | | | | | | | | | | | |
| 13_1 | 5.82E–06 | 2.30E–03 | 1.65E–04 | 7.71E–03 | 1.2714 | 0.0486 | 0.1311 | 0.0062 | 0.6158 | 0.0702 | 0.0014 | 833 | 22 | 794 | 35 | 934 | 42 |
| 13_2 | 7.87E–06 | 2.92E–03 | 2.08E–04 | 1.25E–02 | 0.9831 | 0.0334 | 0.0991 | 0.0056 | 0.8280 | 0.0708 | 0.0021 | 695 | 17 | 609 | 33 | 952 | 61 |
| 21_1 | 6.01E–06 | 8.86E–03 | 5.69E–04 | 3.69E–02 | 0.8952 | 0.0409 | 0.1058 | 0.0039 | 0.3992 | 0.0614 | 0.0007 | 649 | 22 | 648 | 23 | 654 | 26 |
| 31_1 | 3.26E–06 | 2.37E–03 | 1.46E–04 | 1.00E–02 | 0.8291 | 0.0220 | 0.1044 | 0.0017 | 0.3073 | 0.0581 | 0.0009 | 613 | 12 | 640 | 10 | 533 | 36 |
| 31_2 | 5.64E–06 | 5.55E–03 | 3.58E–04 | 2.31E–02 | 0.9024 | 0.0349 | 0.1031 | 0.0047 | 0.5883 | 0.0617 | 0.0006 | 653 | 19 | 633 | 27 | 664 | 22 |
| 31_3 | 1.24E–05 | 8.29E–03 | 5.64E–04 | 3.50E–02 | 0.9503 | 0.1156 | 0.1070 | 0.0113 | 0.4352 | 0.0652 | 0.0011 | 678 | 60 | 655 | 66 | 781 | 35 |
| M213 | | | | | | | | | | | | | | | | | |
| _20_1 | 4.73E–06 | 5.91E–03 | 1.08E–03 | 5.56E–03 | 11.2340 | 0.4710 | 0.4695 | 0.0163 | 0.4152 | 0.1751 | 0.0011 | 2543 | 39 | 2482 | 72 | 2607 | 11 |
| _20_2 | 3.99E–06 | 7.39E–03 | 1.39E–03 | 7.28E–03 | 11.0976 | 0.3352 | 0.4545 | 0.0119 | 0.4348 | 0.1792 | 0.0021 | 2531 | 28 | 2415 | 53 | 2645 | 20 |
| _20_3 | 5.62E–06 | 5.18E–03 | 7.52E–04 | 1.18E–02 | 3.8866 | 0.5875 | 0.2036 | 0.0224 | 0.3633 | 0.1328 | 0.0081 | 1611 | 123 | 1194 | 120 | 2136 | 106 |
| _30_1 | 3.45E–06 | 4.24E–03 | 7.92E–04 | 4.11E–03 | 10.6269 | 0.5348 | 0.4343 | 0.0204 | 0.4678 | 0.1777 | 0.0015 | 2491 | 47 | 2325 | 92 | 2632 | 14 |
| _30_2 | 3.57E–06 | 4.74E–03 | 8.85E–04 | 5.05E–03 | 9.2474 | 0.9764 | 0.3893 | 0.0343 | 0.4177 | 0.1740 | 0.0030 | 2363 | 97 | 2120 | 159 | 2596 | 29 |
| _30_1 | 3.45E–06 | 4.24E–03 | 7.92E–04 | 4.11E–03 | 0.4343 | 0.0204 | 10.6269 | 0.5348 | 0.4678 | 0.1777 | 0.0015 | 366 | 14 | 15815 | 297 | 2632 | 14 |
| _30_2 | 3.57E–06 | 4.74E–03 | 8.85E–04 | 5.05E–03 | 0.3893 | 0.0343 | 9.2474 | 0.9764 | 0.4177 | 0.1740 | 0.0030 | 334 | 25 | 15001 | 616 | 2596 | 29 |
| M164 | [cps] | [cps] | | [cps] | | | | | | | | | | | | | |
| 16_1 | 33 | 38556 | | 680508 | 0.8978 | 0.0256 | 0.1069 | 0.0038 | 0.6230 | 0.0609 | 0.0010 | 651 | 14 | 655 | 22 | 636 | 34 |
| 14_1 | 40 | 21455 | | 387166 | 0.9479 | 0.0363 | 0.1069 | 0.0041 | 0.4970 | 0.0643 | 0.0014 | 677 | 19 | 654 | 24 | 753 | 45 |
| 11_1 | 25 | 31550 | | 562781 | 0.8920 | 0.0248 | 0.1043 | 0.0038 | 0.6516 | 0.0620 | 0.0010 | 647 | 13 | 640 | 22 | 675 | 34 |
| 10_1 | 31 | 14518 | | 275264 | 0.8427 | 0.0268 | 0.1028 | 0.0040 | 0.6085 | 0.0595 | 0.0012 | 621 | 15 | 631 | 23 | 585 | 42 |
| 7_1 | 28 | 94207 | | 1727692 | 0.8539 | 0.0230 | 0.1030 | 0.0038 | 0.6858 | 0.0601 | 0.0008 | 627 | 13 | 632 | 22 | 607 | 29 |
| 6_1 | 32 | 41975 | | 785230 | 0.8402 | 0.0228 | 0.0994 | 0.0036 | 0.6661 | 0.0613 | 0.0010 | 619 | 13 | 611 | 21 | 649 | 35 |

**Table 1** (continued)

| | Final blank corrected intensities (in V) | | | | Final mass bias corrected ratios | | | | | | | Calculated ages | | | | | |
|---|---|---|---|---|---|---|---|---|---|---|---|---|---|---|---|---|---|
| | $^{204}Pb$ | $^{206}Pb$ | $^{207}Pb$ | $^{238}U$ | $^{207}Pb/^{235}U$ | 2σ | $^{206}Pb/^{238}U$ | 2σ | Rho | $^{207}Pb/^{206}Pb$ | 2σ | $^{207}Pb/^{235}U$ | 2σ | $^{206}Pb/^{238}U$ | 2σ | $^{207}Pb/^{206}Pb$ | 2σ |
| 5_1 | 32 | 60529 | | 1120004 | 0.8455 | 0.0211 | 0.1011 | 0.0037 | 0.7317 | 0.0607 | 0.0009 | 622 | 12 | 621 | 22 | 627 | 31 |
| 3_1 | 28 | 31491 | | 560299 | 0.9039 | 0.0290 | 0.1052 | 0.0039 | 0.5841 | 0.0623 | 0.0011 | 654 | 15 | 645 | 23 | 686 | 39 |
| MONAZITES | | | | | | | | | | | | | | | | | |
| TZ69 | | | | | | | | | | | | | | | | | |
| _7_a | 9.87E–07 | 1.88E–02 | 7.52E–04 | 3.71E–01 | 0.7280 | 0.0964 | 0.0896 | 0.0118 | 0.4972 | 0.0581 | 0.0003 | | | | | | |
| _3_c | 2.70E–06 | 1.03E–02 | 4.34E–04 | 2.12E–01 | 0.7770 | 0.0789 | 0.0909 | 0.0097 | 0.5253 | 0.0601 | 0.0007 | | | | | | |
| _9_b | 1.69E–06 | 1.02E–02 | 4.21E–04 | 2.03E–01 | 0.7632 | 0.1460 | 0.0920 | 0.0159 | 0.4512 | 0.0603 | 0.0021 | | | | | | |
| _2_b | 1.28E–06 | 9.39E–03 | 3.84E–04 | 1.81E–01 | 0.8083 | 0.0827 | 0.0950 | 0.0099 | 0.5111 | 0.0604 | 0.0010 | | | | | | |
| _4_a | 2.72E–06 | 1.34E–02 | 5.67E–04 | 2.68E–01 | 0.7751 | 0.0603 | 0.0931 | 0.0069 | 0.4769 | 0.0606 | 0.0006 | | | | | | |
| _1_a | 3.36E–06 | 6.92E–03 | 6.61E–04 | 1.81E–01 | 0.7582 | 0.1152 | 0.0906 | 0.0108 | 0.3923 | 0.0610 | 0.0043 | | | | | | |
| _7_c | 1.25E–06 | 4.78E–03 | 2.05E–04 | 9.37E–02 | 0.7656 | 0.1085 | 0.0895 | 0.0112 | 0.4425 | 0.0615 | 0.0023 | | | | | | |
| _7_b | 1.42E–06 | 4.94E–03 | 2.09E–04 | 9.64E–02 | 0.7646 | 0.0728 | 0.0898 | 0.0081 | 0.4725 | 0.0615 | 0.0009 | | | | | | |
| _6_a | 1.63E–06 | 1.16E–02 | 4.74E–04 | 2.31E–01 | 0.8346 | 0.1623 | 0.0974 | 0.0166 | 0.4372 | 0.0617 | 0.0036 | | | | | | |
| _8_b | 1.90E–06 | 1.08E–02 | 4.48E–04 | 2.12E–01 | 0.8184 | 0.0753 | 0.0963 | 0.0085 | 0.4777 | 0.0621 | 0.0011 | | | | | | |
| _6_b | 1.12E–06 | 5.49E–03 | 2.30E–04 | 1.06E–01 | 0.7890 | 0.0985 | 0.0904 | 0.0116 | 0.5148 | 0.0623 | 0.0014 | | | | | | |
| _4_b | 1.47E–06 | 8.60E–03 | 3.61E–04 | 1.66E–01 | 0.7448 | 0.0643 | 0.0881 | 0.0076 | 0.4979 | 0.0623 | 0.0009 | | | | | | |
| _9_a | 1.70E–06 | 4.91E–03 | 2.13E–04 | 9.66E–02 | 0.8871 | 0.4156 | 0.1035 | 0.0640 | 0.6601 | 0.0635 | 0.0021 | | | | | | |
| _3_b | 3.26E–06 | 6.43E–03 | 2.83E–04 | 1.28E–01 | 0.8529 | 0.1295 | 0.0952 | 0.0145 | 0.5025 | 0.0638 | 0.0012 | | | | | | |
| _5_b | 2.31E–06 | 4.19E–03 | 1.85E–04 | 8.14E–02 | 0.8553 | 0.1870 | 0.0970 | 0.0220 | 0.5188 | 0.0640 | 0.0013 | | | | | | |
| _5_a | 1.87E–06 | 8.09E–03 | 3.39E–04 | 1.57E–01 | 0.8605 | 0.0877 | 0.0982 | 0.0092 | 0.4577 | 0.0641 | 0.0024 | | | | | | |
| _3_a | 4.02E–06 | 1.38E–02 | 5.77E–04 | 2.76E–01 | 0.8764 | 0.3239 | 0.0981 | 0.0268 | 0.3700 | 0.0645 | 0.0012 | | | | | | |
| _8_a | 1.92E–06 | 6.99E–03 | 3.02E–04 | 1.39E–01 | 0.8734 | 0.1900 | 0.0978 | 0.0183 | 0.4303 | 0.0648 | 0.0035 | | | | | | |
| _2_a | 2.21E–06 | 8.61E–03 | 3.61E–04 | 1.72E–01 | 0.8611 | 0.1055 | 0.0945 | 0.0113 | 0.4868 | 0.0656 | 0.0033 | | | | | | |
| _1_b | 4.25E–06 | 3.88E–03 | 3.98E–04 | 1.00E–01 | 0.8462 | 0.1273 | 0.0911 | 0.0134 | 0.4904 | 0.0667 | 0.0014 | | | | | | |
| TZ87 | | | | | | | | | | | | | | | | | |
| _01a | 2.62E–06 | 1.93E–03 | 3.09E–04 | 4.27E–03 | 11.0302 | 1.3328 | 0.4477 | 0.0540 | 0.4993 | 0.1749 | 0.0045 | | | | | | |
| _02a | 5.13E–07 | 2.25E–03 | 3.54E–04 | 4.75E–03 | 11.2528 | 0.5166 | 0.4646 | 0.0204 | 0.4784 | 0.1737 | 0.0015 | | | | | | |
| _03a | 5.27E–07 | 2.45E–03 | 3.87E–04 | 5.07E–03 | 11.9908 | 0.8696 | 0.4842 | 0.0321 | 0.4567 | 0.1734 | 0.0030 | | | | | | |
| _04a | 1.90E–06 | 7.09E–03 | 1.11E–03 | 1.41E–02 | 11.5929 | 0.3799 | 0.4817 | 0.0156 | 0.4931 | 0.1736 | 0.0004 | | | | | | |
| _04b | 7.20E–07 | 1.92E–03 | 3.06E–04 | 3.95E–03 | 11.7717 | 1.0577 | 0.4826 | 0.0420 | 0.4847 | 0.1772 | 0.0008 | | | | | | |
| _04c | 4.77E–06 | 5.07E–03 | 7.93E–04 | 1.18E–02 | 11.1802 | 0.5390 | 0.4641 | 0.0219 | 0.4891 | 0.1735 | 0.0021 | | | | | | |
| _05a | 2.73E–06 | 2.59E–03 | 1.45E–04 | 3.04E–02 | 0.7324 | 0.4202 | 0.0864 | 0.0370 | 0.3730 | 0.0638 | 0.0572 | | | | | | |
| _05b | 3.32E–06 | 1.51E–03 | 2.47E–04 | 3.44E–03 | 11.0907 | 0.7600 | 0.4415 | 0.0279 | 0.4610 | 0.1805 | 0.0030 | | | | | | |
| _05c | 5.37E–07 | 2.56E–03 | 1.35E–04 | 2.81E–02 | 0.7306 | 0.0967 | 0.0906 | 0.0119 | 0.4944 | 0.0584 | 0.0004 | | | | | | |
| _05d | 5.20E–05 | 3.67E–03 | 5.74E–04 | 3.36E–02 | 2.3375 | 1.6910 | 0.1196 | 0.0444 | 0.2566 | 0.1430 | 0.0738 | | | | | | |
| _05e | 2.45E–06 | 3.48E–03 | 5.54E–04 | 7.80E–03 | 10.9154 | 8.8449 | 0.4453 | 0.2481 | 0.3438 | 0.1743 | 0.0523 | | | | | | |

**Table 2** U-Pb analytical results from measuring campaigns using the SIMS (Nordsim) in Stockholm

SIMS U-Th-Pb data and derived ages

| Grain/spot | Concentration (ppm) | | Th/U | $^{206}Pb/^{204}Pb$ | $f_{206}$ (%) | Isotope ratio±σ(%) | | | | Age±σ(%) | |
|---|---|---|---|---|---|---|---|---|---|---|---|
| | U | Pb | | | | $^{207}Pb^*/^{206}Pb^*$ | $^{207}Pb/^{206}Pb_{raw}$ | $^{206}Pb^*/^{238}U$ | $^{206}Pb/^{238}U_{raw}$ | $^{207}Pb/^{206}Pb$ | $^{206}Pb/^{238}U$ |
| TV02_78—Orthogneiss Kiboriani Mountains | | | | | | | | | | | |
| g2-1 | 38 | 27 | 1.079 | 42109 | 0.04 | 0.17481±1.06 | 0.17510±1.05 | 0.48390±3.09 | 0.48390±3.09 | 2604±18 | 2544±65 |
| g35-1 | 38 | 27 | 0.949 | 11407 | 0.16 | 0.17603±1.07 | 0.17711±1.04 | 0.48313±3.08 | 0.48313±3.08 | 2616±18 | 2541±65 |
| g4-1 | 32 | 21 | 0.746 | 19139 | 0.10 | 0.17371±1.09 | 0.17435±1.07 | 0.47336±3.20 | 0.47336±3.20 | 2594±18 | 2498±67 |
| g34-1 | 41 | 30 | 1.135 | 23126 | 0.08 | 0.17906±1.11 | 0.17950±1.10 | 0.48657±3.80 | 0.48657±3.80 | 2644±18 | 2556±66 |
| TV02_51—Orthogneiss Nguru Mountains | | | | | | | | | | | |
| g7-1 | 1157 | 343 | 0.189 | 38027 | 0.05 | 0.12008±0.54 | 0.12043±0.54 | 0.24770±3.08 | 0.24770±3.08 | 1957±10 | 1427±40 |
| g7-2 | 159 | 16 | 0.033 | 6854 | [0.27] | n/a | 0.06801±1.48 | n/a | 0.09287±3.10 | 869±31 | 573±17 |
| g8-1 | 1142 | 230 | 0.063 | 12510 | 0.15 | 0.10787±0.48 | 0.10900±0.46 | 0.17685±3.21 | 0.17685±3.21 | 1764±9 | 1050±31 |
| g4_1 | 1016 | 382 | 0.819 | 54154 | 0.03 | 0.12185±0.29 | 0.12210±0.29 | 0.26035±1.65 | 0.26035±1.65 | 1984±5 | 1492±22 |
| g5_1 | 1019 | 323 | 0.650 | 7760 | 0.24 | 0.11862±0.42 | 0.12035±0.37 | 0.22477±1.67 | 0.22477±1.67 | 1936±8 | 1307±20 |
| g13_1 | 1764 | 597 | 0.178 | 203414 | 0.01 | 0.12739±0.14 | 0.12746±0.14 | 0.28300±1.65 | 0.28300±1.65 | 2062±3 | 1606±24 |
| C58—Grt-Amphibolite Western Granulites | | | | | | | | | | | |
| g25_1 | 165 | 63 | 0.350 | 12809 | 0.15 | 0.12425±0.54 | 0.12529±0.52 | 0.30865±1.65 | 0.30910±1.65 | 2018±10 | 1734±25 |
| g40_1 | 478 | 191 | 0.476 | 53565 | 0.03 | 0.11653±0.31 | 0.11678±0.30 | 0.31548±1.66 | 0.31559±1.66 | 1904±6 | 1768±26 |
| g7_1 | 476 | 197 | 0.354 | 34429 | 0.05 | 0.11744±0.31 | 0.11783±0.30 | 0.33977±1.67 | 0.33995±1.67 | 1918±6 | 1886±27 |
| g7_2 | 1225 | 408 | 0.341 | 48514 | 0.04 | 0.11683±0.34 | 0.11710±0.34 | 0.26835±1.65 | 0.26845±1.65 | 1908±6 | 1532±22 |
| g18-1 | 1291 | 458 | 0.476 | 54501 | [0.03] | n/a | 0.11634±0.36 | n/a | 0.27587±1.72 | 1901±7 | 1571±24 |
| g19-1 | 70 | 18 | 0.150 | 7459 | [0.25] | n/a | 0.10858±1.05 | n/a | 0.22124±1.74 | 1776±19 | 1288±21 |
| g16-1 | 661 | 256 | 0.319 | 91547 | [0.02] | n/a | 0.11713±0.28 | n/a | 0.31858±1.71 | 1913±5 | 1783±27 |
| g14-1 | 465 | 193 | 0.516 | 63506 | [0.03] | n/a | 0.11791±0.33 | n/a | 0.32551±1.71 | 1925±6 | 1817±27 |
| g13-1 | 700 | 223 | 0.192 | 62902 | [0.03] | n/a | 0.11425±0.34 | n/a | 0.26925±1.71 | 1868±6 | 1537±24 |

$f_{206}$(%) is the amount of common $^{206}$Pb, estimated from measured $^{204}$Pb. Values in paraentheses indicate that the $^{204}$Pb count was not significantly higher than detector background and in these cases, where common Pb correction has been applied, we do not report corrected $^{206}Pb/^{238}U$ and $^{207}Pb/^{206}Pb$ ratios (indicated by n/a in those columns). Th/U ratios are calculated from measured ThO/U ratios relative to the standard

Tanzania Craton are Archean (2.7–3.5 Ga) with a metamorphic imprint around 2.5 Ga (Pinna 1996; Bellucci et al. 2011). The protolith formation ages of the Usagaran magmatic rocks cluster around 2.0 Ga. In the southern parts of the belt, the Craton margin is bordered by a characteristic Usagaran unit, the sedimentary Konse Group. This unit disappears in the North and cannot be used as distinctive criterion for the occurrence of Usagaran rocks. Here, the margin between the meta-magmatic Craton and a possible occurrence of the meta-magmatic Usagaran Belt is poorly defined. Due to the lack of geochronology data, it is even unclear, if relicts of the Usagaran Belt can be found in the northern areas of Tanzania. A distinction between the two orogenic belts based on structural criteria is also difficult because of pervasive Neoproterozoic deformation and the still-active structural imprint of the East-African rift (see also Bellucci et al. 2011). The Craton Margin in the North is defined by a zone of strong deformation named the "Bubu cataclasites". One approach of this study is to look for possible Usagaran relicts by dating various meta-magmatic and meta-sedimentary samples along the border of the Tanzania Craton. In the following a short description of outcrops, samples and the zircons is given with the individual age results.

TZ10

The sample TZ10 is a Grt-bearing orthogneiss with a migmatitic texture (Fig. 2a). It was taken close to the village Chinangali north of the main road to Dodoma and is part of the boundary zone of the Tanzania Craton that is tectonically reworked. The mineral assemblage is: Qtz – Kfs – Pl – Bt – Ms. Accessories are Ep, Ap and abundant Zrn. Tectonic reworking can be seen by the recrystallization of the feldspar porphyroblasts forming core-mantle textures.

The zircons are elongated to slightly oval shaped euhedral grains with inclusions of Mnz, Qtz and Kfs.

The internal texture of the larger grains shows different growth zones with a central metamict zone that is surrounded by where the crystal is intensely fractured. The intact parts have been used for the laser ablation traces, however it can be seen in the BSE-images, that no distinct magmatic growth zonation (oscillatory growth) is preserved due to a likely diffusional blurring of the initial structure by the fractures (Fig. 6a). Therefore the results of the isotopic ratios are rather poor. Nevertheless, a Discordia can be defined using an Anchoring point at 0 (Fig. 6b). A discordant line cuts the Concordia in the Archean defining a formation age for this rock around 2,939±180 Ma. This rock clearly stems from the magmatic suite of the Tanzania Craton. A $^{207}Pb/^{206}Pb$ mean age is calculated at 2,953± 110 Ma.

TZ28

Within the outer boundary of the Tanzania Craton ("reworked Craton") in the area around the capital Dodoma this outcrop exhibits strongly deformed migmatitic Hbl-bearing gneisses with concordant (to slightly discordant) pegmatites (Fig. 1). The mineral assemblage is defined by Hbl-Pl-Qtz-Kfs-Bt with the growth of low-grade sericite around fractured Pl-clasts (Fig. 4b). Accessory minerals are Ttn and Zrn.

The shape of the zircons is elongated to roundish with a size of ca.200 μm (Fig. 6c). The elongated zircons typically contain magmatic cores with oscillatory zoning seen in the BSE images. Some grains have a metamict core. The core is surrounded by a broad bright rim (in BSE) showing sector zoning that has a very narrow dark band at the very rim of the grains. A concordant age can be constrained at 2,610± 10 Ma for the cores. Using the anchoring method with a fixed age at550±50 an upper intercept is defined at 2,705± 370 Ma. When anchored at 0 the results give 2,584±26 Ma which is taken as the most reliable result and shown in Fig. 6c. A $^{207}Pb/^{206}Pb$ mean age is calculated at 2,579± 23 Ma (Fig. 6c).

TZ85

This sample was also collected within the Craton boundary ("reworked Craton" or "Bubu Cataclasites") close to Kondoa (Fig. 1). It is a meta-magmatic granodiorite with a relict magmatic texture and is slightly foliated by low-grade retrogression (Fig. 2b). This is seen in this section by the formation of fine-grained Ms around Fsp embedded in a matrix of Qtz and Bt (Fig. 4c).

The zircons are elongated crystals with prismatic edges and internal zonation defined by oscillatory growth patterns in BSE (Fig. 6d). This indicates largely magmatic growth responsible for the formation of these zircons. Some grains contain xenocrystic metamict cores with a destroyed crystal lattice.

Despite the magmatic appearance of the zircons most of the data are discordant and indicate an event overprinting the previous magmatic texture (Fig. 6d). Laying a Discordia through an anchoring point of 0 allows the calculation of an upper intercept age of 2,651±79 Ma –an Archean formation age of this magmatic rock from the Craton. $^{207}Pb/^{206}Pb$ mean age calculation gives 2,625±130 Ma (Fig. 6d).

TZ69

The outcrop from which this sample was taken contains a multiply folded Bt-Ms (para)gneiss from the metasedimentary Kelema Group close to the Craton boundary (Fig. 1). The gneiss is partly migmatitic and injected by


**Fig. 2** Outcrop photographs from the different outcrops along the Tanzania Craton margin. **a** A garnet bearing migmatitic gneiss from the Tanzania Craton. **b** Metamorphic granodiorite of the Tanzania Craton. **c**, **d** Magmatic biotite gneiss from the Western Granulites at the margin to the Tanzania Craton. Fold axes trend north–south. **e** Leucocratic Western Granulites gneiss form northern Tanzania

pegmatites and mica growth in folded parts (Fig. 2c). The mineral assemblage is: Qtz – Pl (Ab) – Bt – Ms (Fig. 4d). Accessories are Rt and abundant Zrn and Mnz. Zircon occurs in the matrix and enclosed in Bt. Monazite is predominately incorporated in metamorphic Bt-laths.

The zircons have inclusions of Qtz and Bt. Slightly rounded and corroded oval grains have internal oscillatory growth patterns with occasional fracturing in the internal parts (Fig. 7a). Brighter rims in BSE indicate a later growth phase probably related to a metamorphic event. A Concordia age can be calculated around 2,607±21 Ma (Fig. 7b). The error ellipses of the data are considerably high. An upper intercept age of a discordant line fixed at an age of 584±12 Ma gives a more precise Archean formation age of this rock at 2,637±90 Ma. This anchoring age of 584±12 Ma for the lower intercept was taken from Monazite analyses in the following presented in Fig. 7c,d. A series of profiles were laid across Monazite grains that have been grown around 584±12 Ma and serves as anchoring age for the Zircon calculation (Fig. 7b). No indication for a Usagaran event is conserved in this sample. The $^{207}Pb/^{206}Pb$ mean age of this sample is 2,624±74 Ma.

TZ87

Close to the Craton Boundary, however in the sequences of the Mozambique Belt, this meta-granodiorite was sampled (Fig. 1). The mica-bearing felsic rock with the assemblage

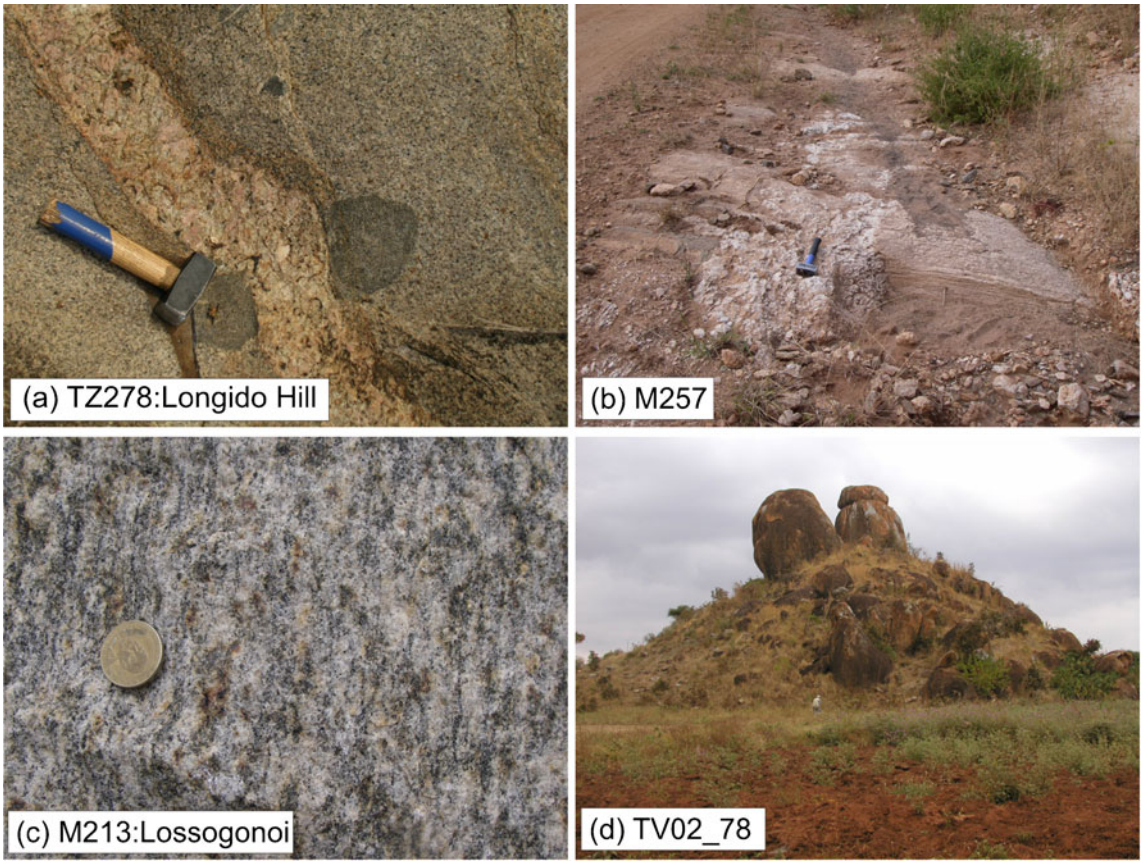


**Fig. 3** Outcrop photographs from the different outcrops from the Maasai Steppe and the Kiboriani Shear Belt. **a** Porphyroblastic orthogneiss with mafic xenolite cut by pegmatite (Eastern Granulites, north Tanzania). **b** Pegmatite crosscutting a sequence biotite gneises containing Amph-boudins. **c** Migmatitic, garnet-bearing orthogneiss at the base of Lossogonoi Mountain (Fig. 1). **d** Meta-tonalitic gneiss from northern margin of Kiboriani Mountains (Fig. 1)

Bt-Ms-Kfs-Pl-Qtz has a well defined augengneiss texture (Fig. 4e). The mineral assemblage is rich in Zircon and Monazite abundantly grown within the Bt-Ms-foliation forming intergrowth textures. The contrast of the BSE image in Fig. 4e does not allow a distinction between Zrn and Mnz. Therefore two small inserts of Zrn grains have been added with a different contrast showing the internal pattern of the Zrn with bright Mnz grains in and around the Zrn. Even better visible is the relation between Zrn and Mnz forming complex growth patterns in the detailed BSE images (Fig. 7e,g). There are two generations of zircon and two generations of monazite.

The first zircon generation is defined by thin elongated prismatic grains (length: 200–300 μm) with magmatic internal structures indicated by dominant osciallatory zoning and occasional formation of sector patterns (Fig. 7e). Metamict cores and zones are frequently found. This causes the problem in this sample that the data quality is poor and the analysed spots plot quite off the Concordia making it impossible to calculate an upper intercept age (Fig. 7f). Only two spots plot at the Concordia and give a concordant Archean age at 2,653±41 Ma. The second Zrn generation is found in and around larger monazite grains. From those grains no analyses could be made.

The monazite analyses allow the calculation of more well-defined ages. Large grains of the first generation are probably of magmatic origin and the analysed data points allow calculation an upper intercept age at 2,610±44 Ma. Analyses of small Mnz grains (often grown around the first Zrn generation) give a lower intercept at 555±80 Ma. When calculated as concordant ages the older Mnz generation has an age of 2,556±10 Ma and the younger grains have an age of 556±26 Ma (Fig. 7h).

TZ89

This sample is a Bt-bearing gneiss from the road Kondoa—Kibaya close to the Tanzania Craton (Fig. 1). The mineral assemblages is Qtz – Kfs – Pl –Bt (Fig. 4f). Accessory minerals are Ttn, Zrn and Fe-Oxides.

The zircons are mainly elongated prismatic grains (up to 500 μm length) with complex zoning patterns (Fig. 8a). A typical observation is the growth of zircon twins. The internal structure of the zircon grains is characterised by a couple

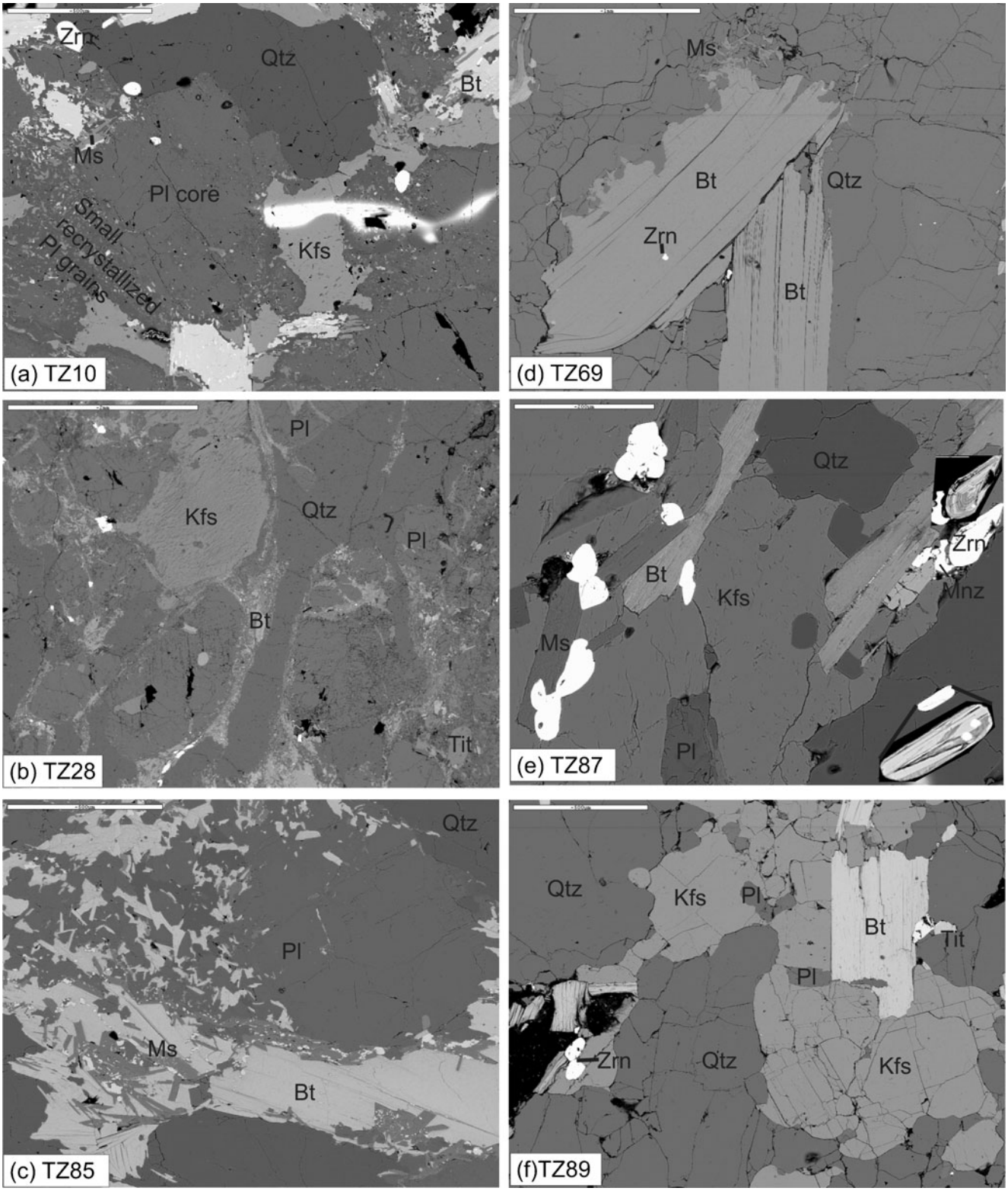


**Fig. 4** Mineral assemblages made with backscattered electron microscopy from the Craton Margin samples (sample localities see Fig. 1; GPS positions see the various diagrams Figs. 6, 7, 8, 9, 10). **a** TZ10: Migmatitic orthogneiss showing tectonic reworking textures in the mineral assemblage. **b** TZ28: Migmatitic orthogneiss found close to Dodoma. Serizite is found around fractured feldspar, a typical feature of the "reworked Craton" boundary. **c** TZ85: Meta-granodiorite found along the Craton Margin north of Dodoma. **d** TZ69: Paragneiss from the meta-sedimentary Kelema Group close to the Craton boundary. **e** TZ87: Metagranodiorite with augengneiss texture and abundant Zrn and Mnz in the foliation. Two inserts were made of larger Zrn grains with a different contrast to clarify the relation between Zrn and Mnz. **f** TZ89: Bt-gneiss collected close to the Craton boundary

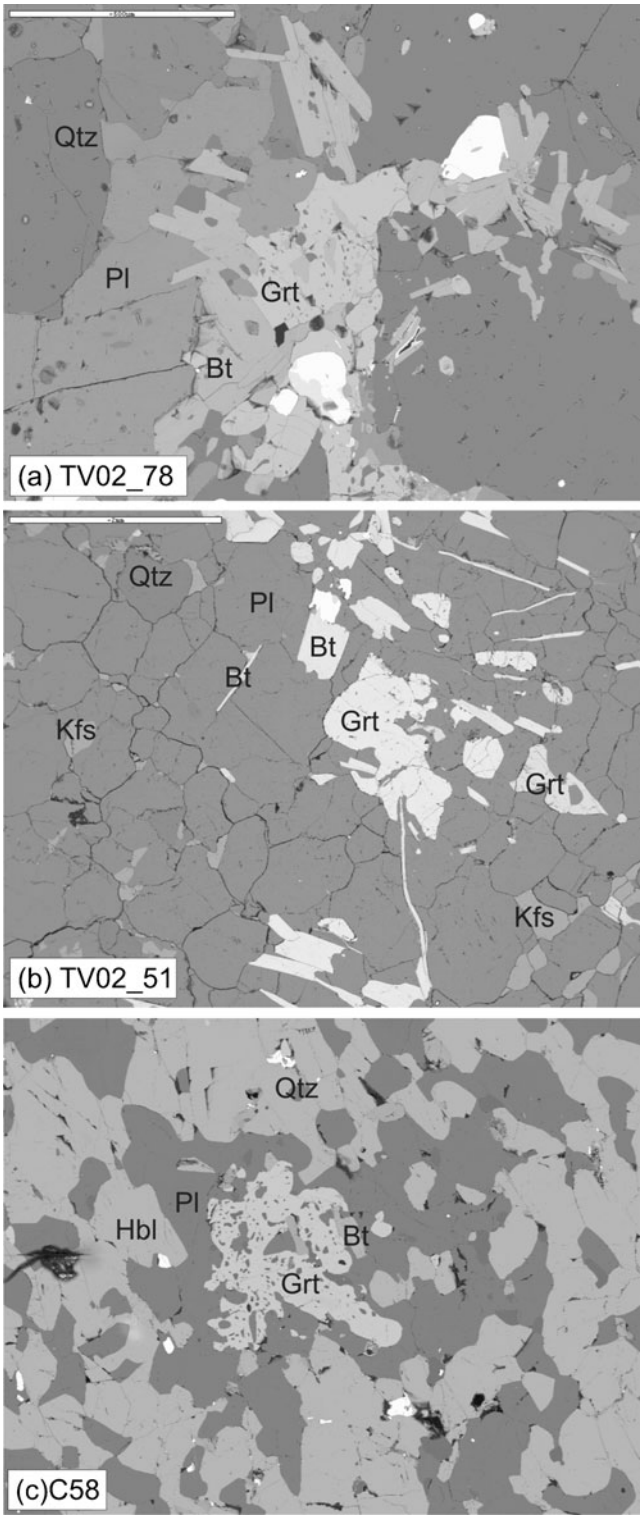


**Fig. 5** Mineral assemblages from the analysed samples of the basement-cover chapter made with backscattered electron microscopy. (sample localities see Fig. 1; GPS positions see the various diagrams Figs. 6, 7, 8, 9, 10). **a** TV02_78: Tonalitic gneiss from the Kiboriani Mountains with poikilitic garnet. **b** TV02_51: Garnet bearing tonalitic gneiss from the Nguru Mountains. **c** Amphibolite from the Western granulites showing the typical metamorphic decompression texture of Pl rims around Grt

of separate zones outlined in Fig. 8a. There are xenocrystic cores (I) with lobate patterns surrounded by a zone of brighter reflection in BSE (II). This zone is partly fractured or has a destroyed lattice of metamict zircon. The outlined geometry resembles an elongated prismatic idiomorphic crystal. A third zone (III) corresponds to a broader growth phase with sector zoning. The outermost rim shows oscillatory patterns and is corroded at the crystal edges giving a subrounded shape. The ablated profiles lie in zones II and III and the analysed data points plot in the diagram close to the Concordia around 2.6 Ga (Fig. 8b). The discordant data points indicate a subsequent overprint around 550±50 Ma. Using this anchoring spot an upper intercept age can be calculated at 2,697±55 Ma.

TZ95

This fine-grained Bt-gneiss is sampled along the road from Kondoa to Kibaya—some distance away from the Craton Margin towards the Maasai Steppe (Fig. 1).

Inclusions in Zircons are Ap. The internal structure of the Zircon grains is complex as seen in Fig. 8c. There are small idiomorphic xenocrystic cores showing sector zoning. These are surrounded by a fractured metamict zone followed by a subsequent growth zone with a broader metamorphic rim. The analysed spots plot in the diagram as a cluster through which a Discordia can be laid (Fig. 8d). The upper intercept gives an age of 2,677±110 Ma and a lower intercept is calculated around 50 Ma±780 Ma. When anchoring the Discordia at 0 a better defined upper intercept age can be calculated at 2,722±55 Ma (Fig. 8d). The $^{207}Pb/^{206}Pb$ mean age of this sample is 2,702±48 Ma (Fig. 8d).

TZ93

This sample was taken in the sequences of the Mozambique Belt some distance away from the Craton margin (Fig. 1). It consists of highly-deformed and recrystallised migmatitic banded gneisses and has a W-E trending layering, dipping to the south (Fig. 2d).

Most zircon grains are elongated, prismatic with subrounded edges, having a length of ca. 200 μm (Fig. 8e). From the complex internal structure four growth zones can be inferred (Fig. 8e): The small internal core (zone I) has a moderately elongated prismatic shape. The BSE pattern of this core is characterised by sector zoning to broad oscillatory zoning. Diffusive processes formed lobate structures growing into the core. The second zone surrounding the core (zone II) is a broad metamict part, where the crystal lattice is destroyed. This metamict zone has an elongated ellipsoid shape and fills a considerable volume of the zircon grain. The next zone (III) is blurry shaded starting with a darker grey (BSE pattern) at the boundary to zone II and

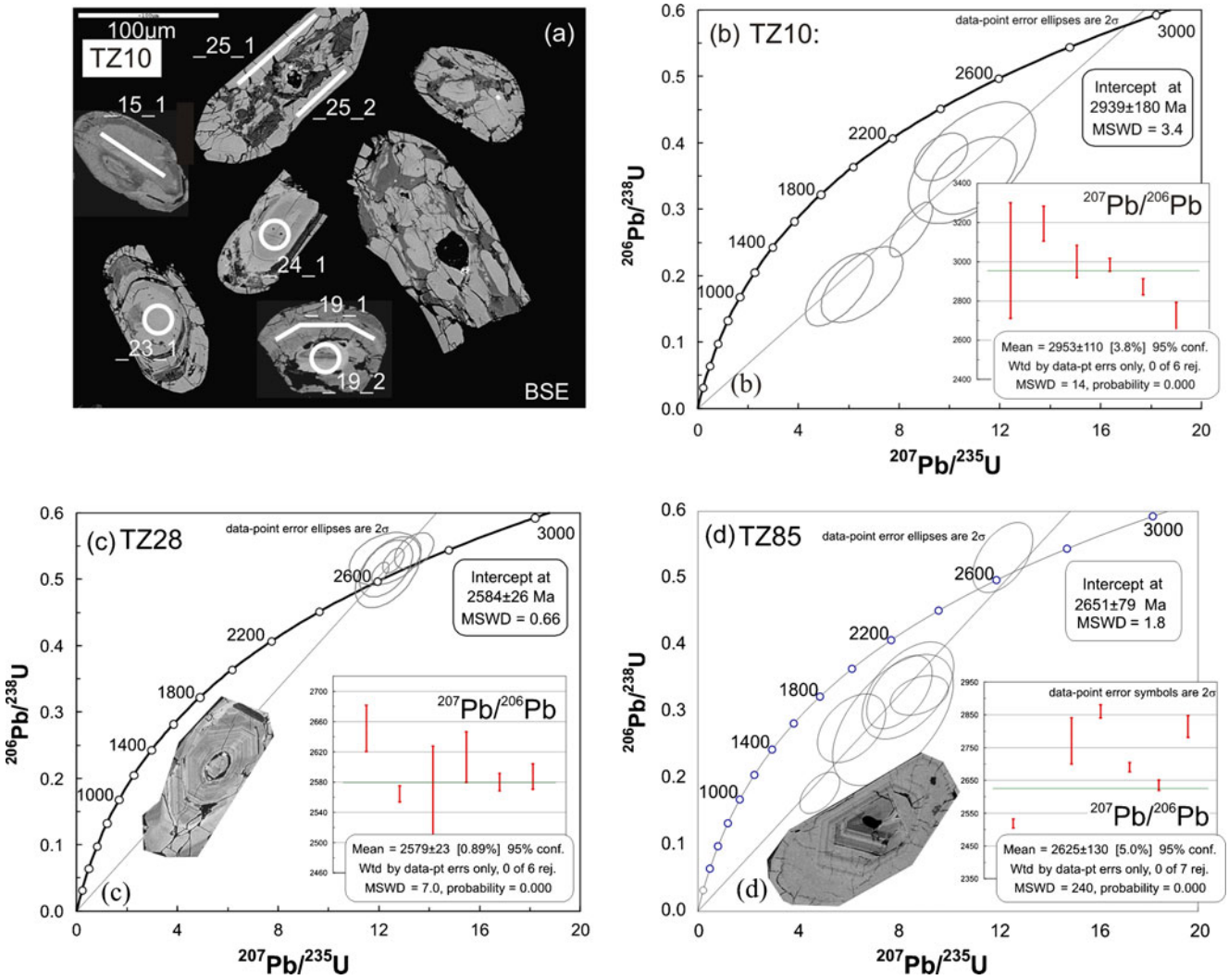


**Fig. 6** Microphotographs (Scanning electron microscopy) displaying internal zircon textures and the according geochronological results shown in the conventional Concordia diagrams. Datapoint error ellipses are 2σ. The samples are representing the Craton Margin. The abbreviations: BSE=images made by backscattered electron microscopy; CL=images made by Cathodoluminescence microscopy. The white dashed lines and circles indicate the analysed parts of the zircon were laser ablation was applied. **a** BSE image from orthogneiss sample TZ10 with the ablated spots and profiles outlined. **b** The corresponding conventional Concordia diagram for sample TZ10. **c** Diagram for the migmatitic gneiss TZ28. The inserted zircon grain shows the internal texture in BSE and has a length of 200 µm **d** Sample TZ85 from the reworked Craton. The inserted zircon grain shows the internal texture in BSE and has a length of 200 µm

getting brighter towards the rim of the zircon. At the ultimate rim a small zone (IV) can be separated from the others by a couple of oscillatory stripes that form a regular, despite very narrow prismatic shape around zone III. Parts of zone IV are detached by later corrosion.

Apart from the igneous zircons some grains are found that are smaller and rounded showing only the internal pattern of zone III. These are interpreted as metamorphic grains.

In the Concordia plot two spots from the core (zone I) display a Concordia Age=2,760±44 Ma. Two metamorphic grains (with zone III) plot at the Concordia around 2,492±

**Fig. 7** Microphotographs (Scanning electron microscopy) displaying ▶ internal zircon textures and the according geochronological results shown in the conventional Concordia diagrams. Datapoint error ellipses are 2σ. **a** BSE image of the zircons from sample TZ69. **b** Concordia diagram with the analysed zircon ages of sample TZ69. **c** BSE image of the analysed monazite grains from sample TZ69. **d** Concordia diagram with the monazite ages plotted. **e** Internal structures of the zircons from sample TZ 87 with monazite inclusions and monazite grains overgrowing at the rim of the zircons shown as BSE image. The insert gives a detailed image of a monazite grain with a zircon at the rim. **f** Zircon ages of TZ 87 plotted in a Concordia diagram. **g** Monazite grains of sample TZ87 shown as BSE image. **h** Concordia diagram with the monazite ages from sample TZ87

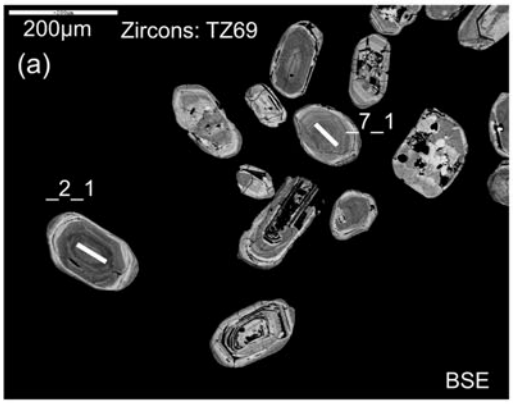
200μm
Zircons: TZ69
(a)
_7_1
_2_1
BSE

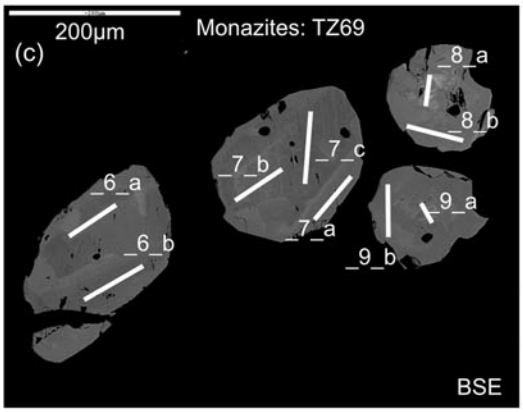
200μm
Monazites: TZ69
(c)
_8_a
_8_b
_7_b
_7_c
_6_a
_6_b
_7_a
_9_a
_9_b
BSE

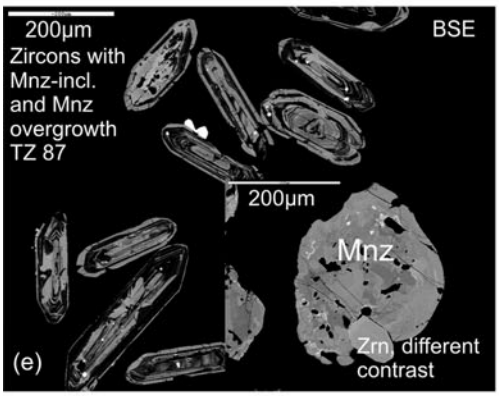
200μm
Zircons with Mnz-incl. and Mnz overgrowth TZ 87
BSE
200μm
Mnz
Zrn, different contrast
(e)

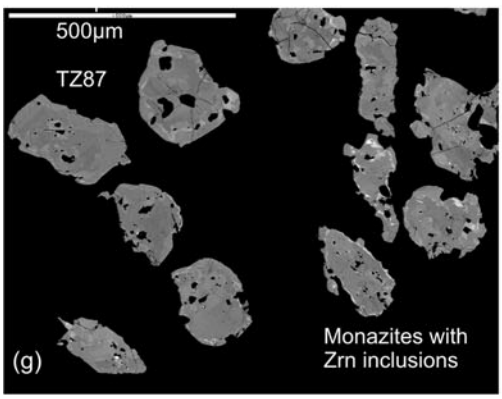
500μm
TZ87
Monazites with Zrn inclusions
(g)

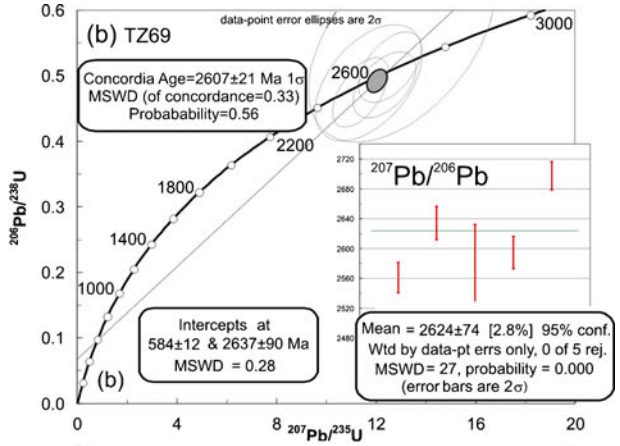
(b) TZ69
data-point error ellipses are 2σ
Concordia Age=2607±21 Ma 1σ
MSWD (of concordance=0.33)
Probability=0.56
Intercepts at
584±12 & 2637±90 Ma
MSWD = 0.28
207Pb/206Pb
Mean = 2624±74 [2.8%] 95% conf.
Wtd by data-pt errs only, 0 of 5 rej.
MSWD = 27, probability = 0.000
(error bars are 2σ)
206Pb/238U
207Pb/235U

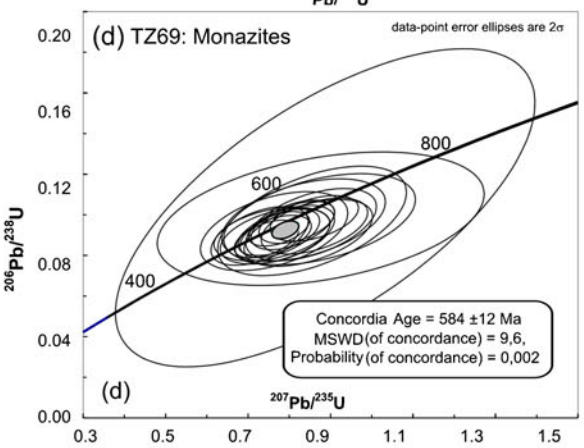
(d) TZ69: Monazites
data-point error ellipses are 2σ
Concordia Age = 584 ±12 Ma
MSWD(of concordance) = 9,6,
Probability(of concordance) = 0,002
206Pb/238U
207Pb/235U

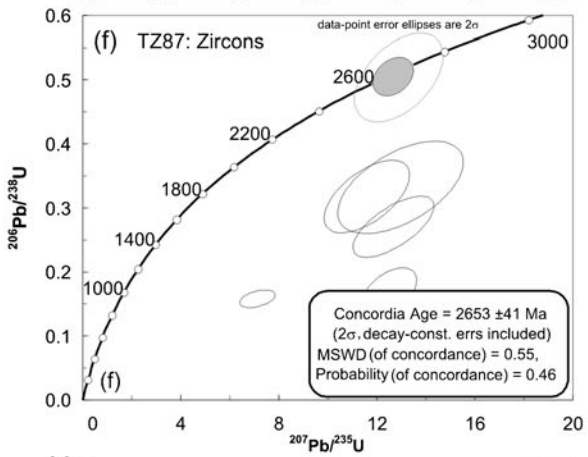
(f) TZ87: Zircons
data-point error ellipses are 2σ
Concordia Age = 2653 ±41 Ma
(2σ, decay-const. errs included)
MSWD(of concordance) = 0.55,
Probability(of concordance) = 0.46
206Pb/238U
207Pb/235U

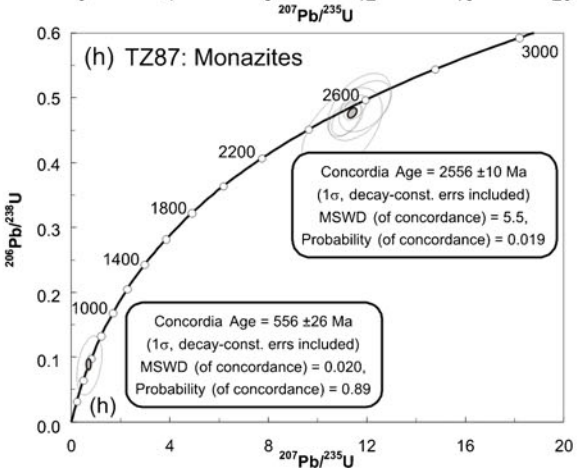
(h) TZ87: Monazites
Concordia Age = 2556 ±10 Ma
(1σ, decay-const. errs included)
MSWD (of concordance) = 5.5,
Probability (of concordance) = 0.019
Concordia Age = 556 ±26 Ma
(1σ, decay-const. errs included)
MSWD (of concordance) = 0.020,
Probability (of concordance) = 0.89
206Pb/238U
207Pb/235U

150 Ma (Fig. 8f). The other spots stem from various parts of zone III from igneous grains plotting along a Discordia with an upper intercept of 2,840±83 Ma. The small rim (zone IV) was too narrow to date, nevertheless indicates a late stage metamorphic overprint. The $^{207}Pb/^{206}Pb$ mean age of this sample is 2,815±10 Ma (Fig. 8f).

Three different growth events can be inferred from these data. The crystallization age of the magmatic rock is given by the cores (zone I) around 2,800 Ma. A subsequent event led to the destruction of the crystal lattice producing the intermediate metamict zone. This is followed by metamorphism (metamorphic grains—zone III) that occurred around 2,500 Ma. Discordant ages from various parts of zone III indicate a late stage overprint, however the intercept is not well-enough defined to infer an exact age. Also the metamorphic rims from zone IV are too narrow for age dating.

M318

Some distance away from the Craton boundary, this orthogneiss was sampled south of the Lake Manyara close to the village Babati (Fig. 1). The rock contains isoclinal folded pegmatites and has the assemblage Hbl-Qtz-Pl-Bt.

The zircons are slightly rounded to elongated prismatic grains with 300 μm length and well-defined internal growth patterns (Fig. 8g). The CL image shows bright cores with patchy zonation and a well-defined homogenous dark rim. Core and rim analyses are plotted in the diagram allowing the calculation of a Discordia with an upper intercept age at 2,715±85 Ma and a lower intercept age at 363±170 Ma. The lower intercept age must be taken with care due to the extremely large error. It only indicates a younger event overprinting the Archean formation age of this rock. When anchoring the lower intercept at Kuungan times (550±50 Ma) the upper intercept is 2,740±90 Ma (shown in Fig. 8g). The $^{207}Pb/^{206}Pb$ mean age is 2,706±48 Ma (Fig. 8g).

M340

Leucocratic gneisses occur along the road to Serengeti National Park close to Loliondo (Fig. 1). This sample was taken from one of the typical outcrops often found in the steppe in and around the National Park named “kopjes” (Fig. 2e). Some of these kopjes are frequently visited by lion families for their siesta.

The zircons are subrounded idiomorphic grains with magmatic oscillatory patterns with occasional partitioning into sector zoning in the brighter core in the CL images (Fig 8h). All analyses plot along the Concordia and the ones from the cores result in concordant ages around 949±13 Ma (Fig. 8h). The calculations for the rim analyses give concordant ages at 488±33 Ma (not shown). The $^{207}Pb/^{206}Pb$ mean age calculation results in 1,027±41 Ma (Fig. 8h).

**Fig. 8** Microphotographs (Scanning electron microscopy) displaying internal zircon textures and the according geochronological results shown in the conventional Concordia diagrams. Datapoint error ellipses are 2σ. **a** Internal structure of zircons of sample TZ89 as BSE image with different growth zones outlined. **b** Concordia plot of sample TZ89. **c** BSE image of sample TZ95 with the analysed profiles outlined. **d** Concordia plot of sample TZ95. **e** BSE image of sample TZ93 with the internal structures and zones of the zircons outlined. **f** Conventional Concordia diagram with the analysed spots of sample TZ93. **g** Concordia diagram of sample M318 with the CL image of a zircon grain as insert showing the typical texture of the zircons. **h** Concordia diagram of sample M340 with the CL image of a zircon grain as insert showing the typical texture of the zircons

## Summary of results

The majority of investigated zircons have grown during the Archean and thus their history is comparable with the crust formation of the Tanzania Craton in the Archean. The long-lived metamorphic and tectonic history led to internal complex growth patterns found in individual sections of the zircon grains. Archean xenocrystic magmatic cores (2.7–2.9 Ga) are surrounded by zones of metamictisation and fracturing. The process leading to the destruction of the crystal lattice is not known but probably related to post Archean erosion and/or sedimentation of the rocks. Subsequent zircon growth around those cores is often found as idiomorphic oscillatory zoning or sector zoning forming elongated prismatic grains. This growth phase can be related to a tectonic event calculated around 2.625 Ga as weighted mean age. Hints for very high grade metamorphic diffusional processes are not found in the zircon grains. Relicts of the Usagaran orogenic event also could not be found with one exception, the southernmost sample (TZ10), giving an upper intercept age of 2,137±33 Ma. This age however is very vague, as it is based on one spot age with a very large uncertainty. It cannot be taken as a real indication for an Usagaran age. Also the typical late Neoproterozoic to Cambrian ages referred to as the Kuunga Orogeny of Gondwana amalgamation are not frequently found in the zircons. The monazites however do nicely show this metamorphic overprint at around 580 Ma (e.g. sample TZ69). The monazites of sample TZ87 have both, an Archean growth phase and a late Neoproterozoic overprint. Weighted mean ages of the two monazite samples and on zircon sample are 582±48 Ma.

## Sample description and analytical results: the central Maasai Steppe

The distinction between Western and Eastern Granulites is mainly based on lithological differences. Thick marble bearing meta-sediments characterise the Eastern Granulites but are rare in the collage of units that are summarised as the

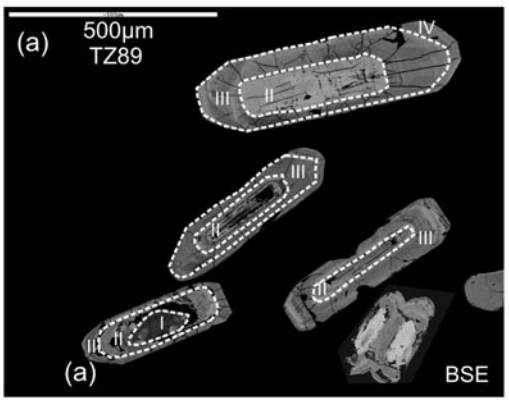
(a)
500µm
TZ89
IV
III
II
I
(a)
BSE

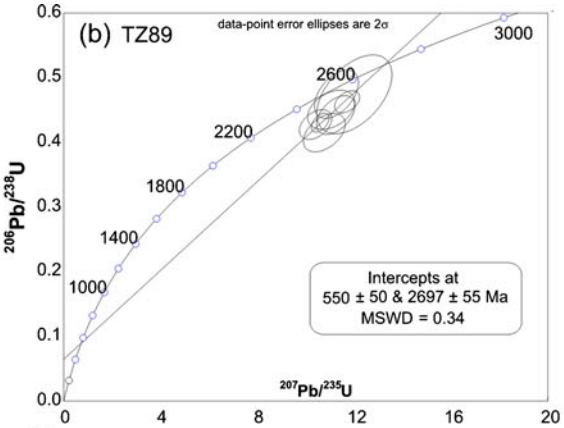
(b) TZ89
data-point error ellipses are 2σ
Intercepts at
550 ± 50 & 2697 ± 55 Ma
MSWD = 0.34
206Pb/238U
207Pb/235U

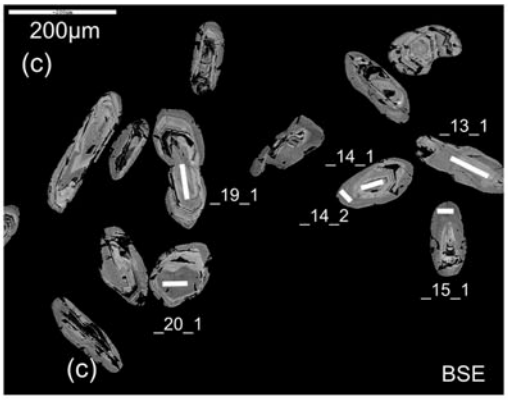
200µm
(c)
_19_1
_13_1
_14_1
_14_2
_15_1
_20_1
(c)
BSE

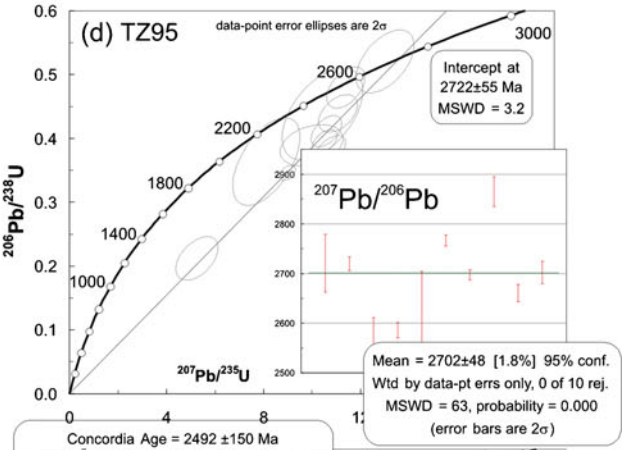
(d) TZ95
data-point error ellipses are 2σ
Intercept at
2722±55 Ma
MSWD = 3.2
207Pb/206Pb
Mean = 2702±48 [1.8%] 95% conf.
Wtd by data-pt errs only, 0 of 10 rej.
MSWD = 63, probability = 0.000
(error bars are 2σ)
206Pb/238U
207Pb/235U

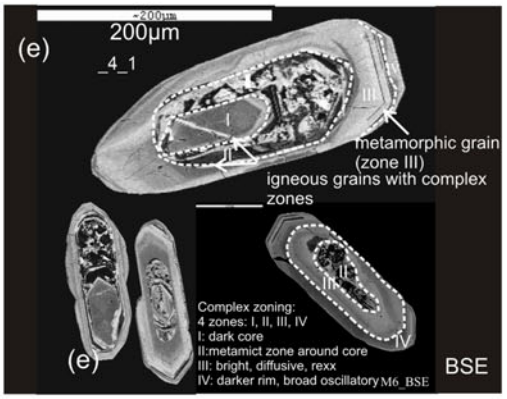
200µm
(e)
_4_1
metamorphic grain
(zone III)
igneous grains with complex
zones
Complex zoning:
4 zones: I, II, III, IV
I: dark core
II:metamict zone around core
III: bright, diffusive, rexx
IV: darker rim, broad oscillatory
(e)
BSE

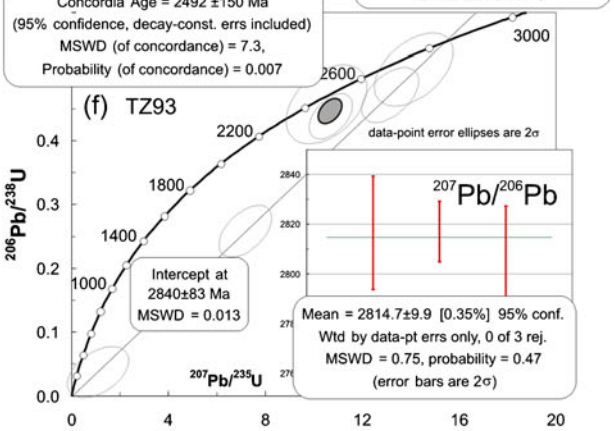
Concordia Age = 2492 ±150 Ma
(95% confidence, decay-const. errs included)
MSWD (of concordance) = 7.3,
Probability (of concordance) = 0.007
(f) TZ93
data-point error ellipses are 2σ
Intercept at
2840±83 Ma
MSWD = 0.013
207Pb/206Pb
Mean = 2814.7±9.9 [0.35%] 95% conf.
Wtd by data-pt errs only, 0 of 3 rej.
MSWD = 0.75, probability = 0.47
(error bars are 2σ)
206Pb/238U
207Pb/235U

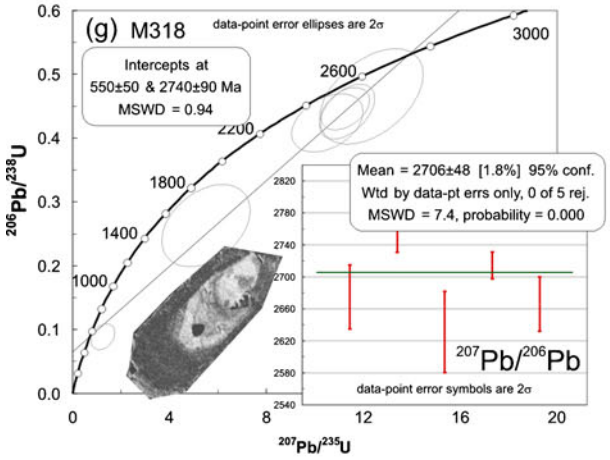
(g) M318
data-point error ellipses are 2σ
Intercepts at
550±50 & 2740±90 Ma
MSWD = 0.94
Mean = 2706±48 [1.8%] 95% conf.
Wtd by data-pt errs only, 0 of 5 rej.
MSWD = 7.4, probability = 0.000
207Pb/206Pb
data-point error symbols are 2σ
206Pb/238U
207Pb/235U

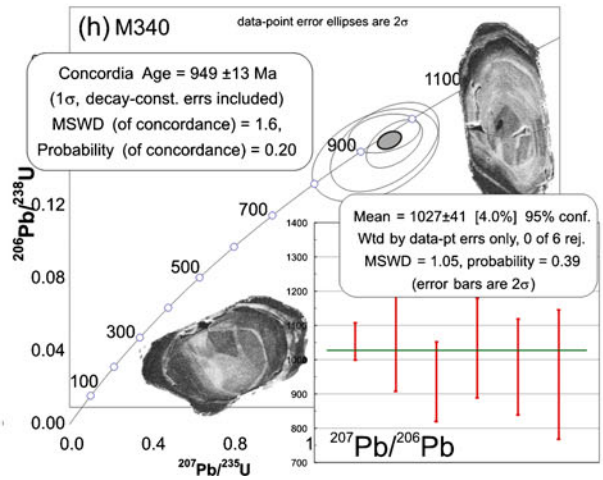
(h) M340
data-point error ellipses are 2σ
Concordia Age = 949 ±13 Ma
(1σ, decay-const. errs included)
MSWD (of concordance) = 1.6,
Probability (of concordance) = 0.20
Mean = 1027±41 [4.0%] 95% conf.
Wtd by data-pt errs only, 0 of 6 rej.
MSWD = 1.05, probability = 0.39
(error bars are 2σ)
207Pb/206Pb
206Pb/238U
207Pb/235U

Western Granulites. In the absence of meta-sedimentary units, however, the distinction becomes vague since both, Western and Eastern Granulites basement units contain granulite facies metamorphosed rocks of similar appearance. In that case the distinction is difficult, especially in the poorly exposed Maasai Steppe, and a proper allocation is mainly based on the investigation of crustal formation ages. In the Western Granulites relicts of Archean (reworked Craton) to 1.8–2.0 Ga ages (reworked Usagaran Belt) are expected. The Eastern Granulites typically have juvenile formation ages around 800–1,000 Ma. General westward thrusting during late Neoproterozoic to Cambrian times created a nappe stack with low-grade metamorphosed Usagaran units in the footwall, highest grade Eastern Granulites in the hangingwall and Western Granulites in between. This situation holds for central Tanzania but is less clear in northern Tanzania (Fig. 1b). Eastern and Western Granulites together have been folded. Dome and basin type fold interference patterns (Fritz et al. 2009; LeGoff et al. 2010) gave rise to inliers of Western Granulites within the Eastern Granulites. In addition complex and poly-phase fold and thrust geometries must be taken into account. Late Neoproterozoic deformation and metamorphism (East African Orogeny) prevails within the Eastern Granulites. Early Cambrian deformation and metamorphism (Kuunga Orogeny), however, has been documented from the Western Granulites (e.g., Cutten et al. 2006) and from the base of the Eastern Granulites at the Uluguru Mountains (Rossetti et al. 2008). In general, this opens the question about extent of East African and Kuunga orogenic phases in general. In this study, a number of key outcrops were chosen with zircon rich samples suitable for geochronology. These are firstly, the large spectacular inselberg mountains (domes) with meta-igneous basement of unknown age and secondly, outcrops showing crucial tectonic features (shear structures and cross-cutting relationships of different tectonic events).

## TZ278

The sample was collected from the Longido Mountain close to the boundary Tanzania to Kenya. Longido Hill is a magmatic body outcropping as inselberg within the surrounding meta-sedimentary rock suites (Fig. 1). The district of Longido is known for the occurrence of ruby in gem quality bound at serpentinised ultramafic bodies within the high-grade metamorphic rocks of the Mozambique Belt. The sample is a coarse-grained porphyroblastic orthogneiss with granitic to tonalitic composition. Post-deformative pegmatites cross-cut the orthogneiss and numerous mafic xenolites occur (Fig. 3a).

The zircons are elongated idiomorphic grains with oscillatory zonation (Fig. 9a). Inclusions are Amph, Pl and Ap.

All analysed spots plot at the diagram (Fig. 9b) as a cluster off the Concordia. Anchoring the lower intercept at 550 Ma an upper intercept age of 2,651±88 Ma is found. The $^{207}Pb/^{206}Pb$ mean age of this sample is 2,563±82 Ma (Fig. 9b).

**Fig. 9** Microphotographs (Scanning electron microscopy) displaying internal zircon textures and the according geochronological results shown in the conventional Concordia diagrams. Datapoint error ellipses are 2σ. **a** CL image of zircons of sample TZ278 from Longido Hill. **b** Concordia diagram of sample TZ278 with age results. **c** Internal texture of the zircons of sample M275 from Lolkisale Hill shown with CL. **d** The results of sample M275 in the Concordia plot. **e** Age data of the pegmatitic sample M257 shown in a conventional Concordia plot. The internal zonation of the zircons is represented by an example as insert (CL-image). **f** Geochronological results of the sample M213 from Lossogonoi Mountain shown in a conventional Concordia plot. The internal zonation of the zircons is shown as CL image. **g** Geochronological results of the sample M164 from a graphite-bearing gneiss in the Lelatema fold shown in a conventional Concordia plot

## M275

This Bt-bearing orthogneiss was sampled in Lolkisale village at the base of Lolkisale Mountain, another meta-magmatic inselberg in the Maasai-Steppe (Fig. 1). The rock is a Grt – Hbl – Bt – Pl – Qtz bearing gneiss with abundant up to 1 mm sized zircons. The quartz and plagioclase matrix is recrystallised and is characterised by 1–2 mm sized equigranular grains. Amphibole is elongated within the foliation planes, 0.5 to 3 mm in size and has a partly poikilitic texture. Biotite occurs either intergrown in amphibole or as elongated flakes within the matrix. Garnet grains have an irregular shape and a size of 1–2 mm and contain inclusions of plagioclase and quartz.

The zircon grains are irregularly rounded and display internal recrystallization textures (Fig. 9c). This is visible from the irregularly zoned dark core surrounded by a bright recrystallised rim with diffusive lobate structures (Fig. 9c). Such zircon textures are typical for granulite facies metamorphism.

The age of this metamorphism however could not be well-constrained by the analyses. The measured spots plot along a Discordia and the intercepts have rather big uncertainties. The formation age of this sample is constrained around 2,551±45 Ma and the lower intercept representing the metamorphic overgrowth is 547±670 Ma. Anchoring the lower intercept at 550 Ma an upper intercept age of 2,551±38 Ma is calculated and shown in Fig. 9d. The $^{207}Pb/^{206}Pb$ mean age of this sample is 2,529±43 Ma (Fig. 9b).

## M257

This key outcrop south of Arusha exposes foliated gneisses (resembling Western Granulites basement) and enderbites (typical for Eastern Granulites basement) that are incorporated into the Lelatema fold system (Fig. 1). The complex

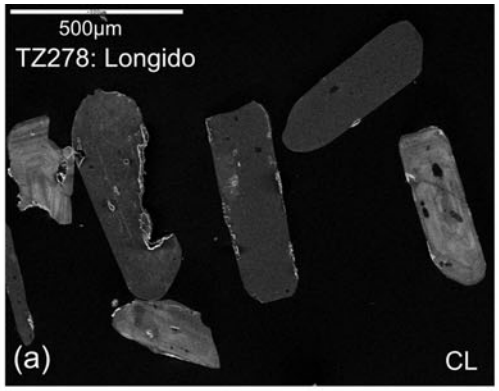
500µm
TZ278: Longido
(a)
CL

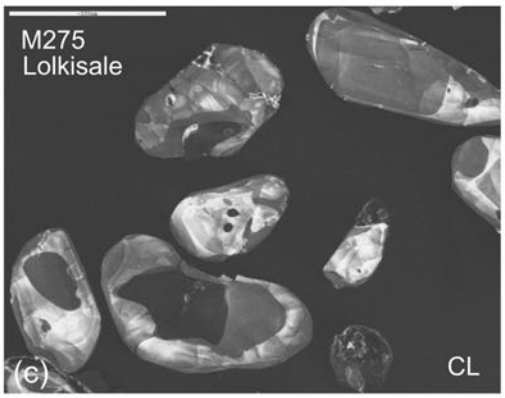
M275
Lolkisale
(c)
CL

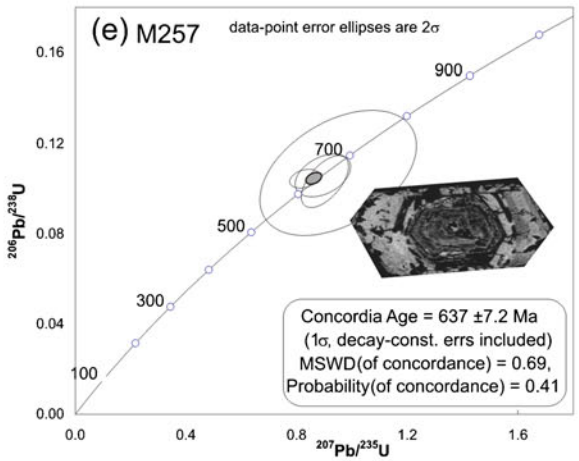
(e) M257
data-point error ellipses are 2σ
Concordia Age = 637 ±7.2 Ma
(1σ, decay-const. errs included)
MSWD(of concordance) = 0.69,
Probability(of concordance) = 0.41
206Pb/238U
207Pb/235U

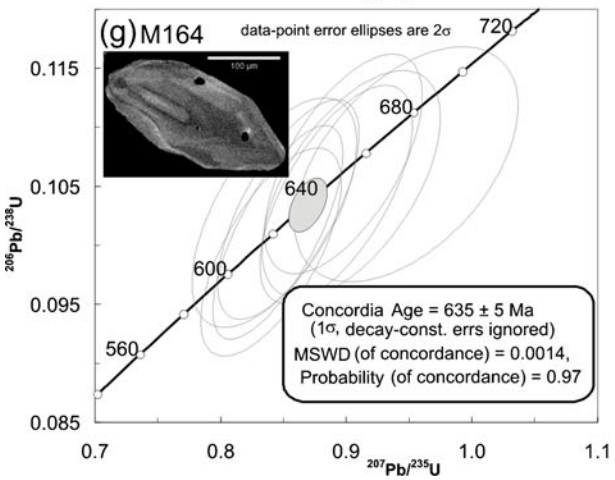
(g) M164
data-point error ellipses are 2σ
Concordia Age = 635 ± 5 Ma
(1σ, decay-const. errs ignored)
MSWD (of concordance) = 0.0014,
Probability (of concordance) = 0.97
206Pb/238U
207Pb/235U

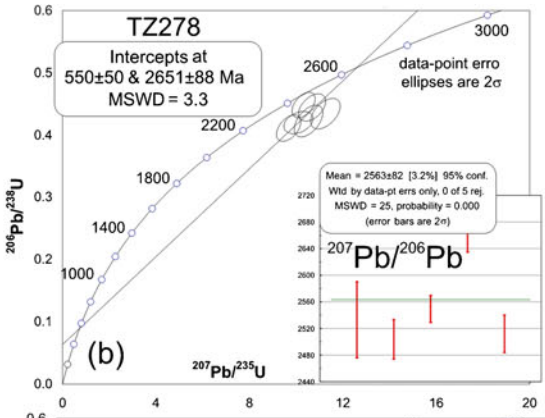
TZ278
Intercepts at
550±50 & 2651±88 Ma
MSWD = 3.3
data-point erro
ellipses are 2σ
(b)
207Pb/206Pb
206Pb/238U
207Pb/235U

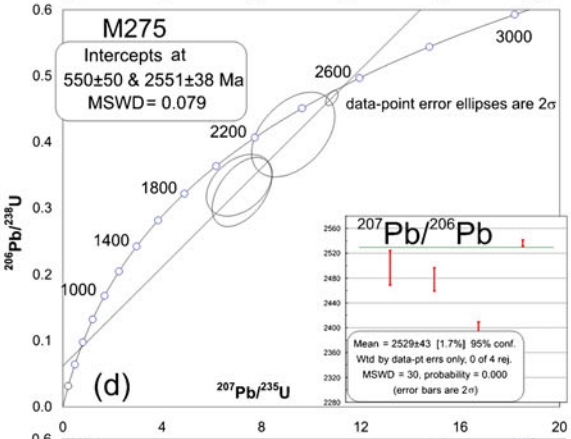
M275
Intercepts at
550±50 & 2551±38 Ma
MSWD= 0.079
data-point error ellipses are 2σ
(d)
207Pb/206Pb
206Pb/238U
207Pb/235U

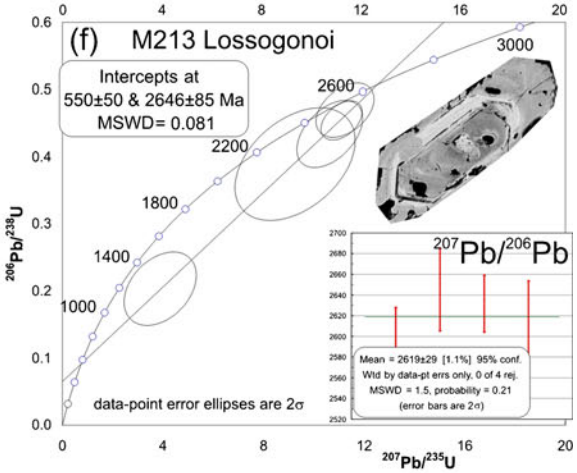
(f) M213 Lossogonoi
Intercepts at
550±50 & 2646±85 Ma
MSWD= 0.081
data-point error ellipses are 2σ
207Pb/206Pb
206Pb/238U
207Pb/235U

structural inventory needs some geochronological background for a better understanding of the tectonic events.

Within a highly sheared sequence of Bt-gneisses including Amph-boudins, voluminous cross-cutting pegmatites can be found (Fig. 3b). The investigated sample is a coarse-grained slightly foliated pegmatitic gneiss consisting of 2–5 mm sized quartz grains which are slightly elongated and show partly straight and partly lobate grain boundaries. Potassium feldspar is slightly altered and up to 5 mm in diameter. Plagioclase is smaller-grained (2–3 mm), contains exsolutions of potassium feldspar and is also slightly altered.

The zircons are elongated prismatic idiomorphic grains (up to 500 μm) with cores showing oscillatory magmatic zoning and metamorphic overgrowth rims as broader zones (Fig. 9e). Two well-defined concordant ages are calculated. The magmatic growth is constrained at 833±22 Ma and the metamorphic age is 637±7 Ma with only the younger age shown in the plot (Fig. 9e).

M213

This migmatitic Grt-bearing orthogneiss was sampled at the base of Lossogonoi Mountain, which is a remarkable inselberg within the core of the Lelatema antiform (Fig. 1). The sample is a coarse-grained slightly foliated granitic gneiss with abundant up to 5 mm large perthitic potassium feldspar, smaller quartz grains and subordinate amounts of plagioclase (Fig. 3c). One to two mm sized garnet, amphibole and biotite grains are distributed within the poorly developed foliation. In addition coronitic reaction textures can be recognised, where a brownish mineral is surrounded by a rim of an orange coloured phase and finally surrounded by potassium feldspars.

Zircon occurs as idiomorphic prismatic grains with rounded edges (Fig. 9f). The size is up to 500 μm and the crystals are rich in inclusions and fractures. The internal structures are predominated by magmatic oscillatory zoning in the core that is partly blurred by diffusion leaving ghost structures. Occasionally metamict xenocrysts are observed. A broad concentrically zoned rim has grown during a metamorphic event of higher grade leading to the element diffusion into the core. Intercepts of a Discordia are recorded at 2,646±100 Ma for the upper intercept and 562±630 Ma. Here again the anchoring method is used for the Kuunga event (550 Ma). The error of the upper intercept decreases then as shown by the result of 2,646±85 Ma (Fig. 9f). The $^{207}Pb/^{206}Pb$ mean age of this sample is 2,619±29 Ma (Fig. 9b).

M164

This sample was collected from a syndeformative pegmatitic layer incorporated into graphitic gneisses that are part of the large Lelatema fold system (Fig. 1). Those graphitic gneisses hosting this Qtz-Fsp rich pegmatite are frequently mined in northern Tanzania for gemstones, e.g. Tsavorite (garnet).

The zircons are large elongated grains (500 μm) with subrounded edges and display internal patterns of oscillatory zoning and sector zonation, partly cut by diffusive lobate zones towards the zircon rim. All measured parts of the zircons give a well-defined Neoproterozoic age of 635±5 Ma in the Concordia diagram (Fig. 9g).

**Fig. 10** Microphotographs (Scanning electron microscopy) displaying internal zircon textures of samples from the Mozambique Belt. The geochronological results are shown in the conventional Concordia diagrams. Datapoint error ellipses are 2σ. **a** CL images of zircons of sample TV02_78 from the Kiboriani Shear Belt. **b** Diagram showing the ages of sample TV02_78. **c** CL images of zircons of sample TV02_51 from the Nguru Shear Belt. **d** Diagram showing the ages of sample TV02_51. **e** C58 is a sample representative for the Western Granulites. The CL image shows the internal texture of the zircons. **f** The age data of C58 in a conventional Concordia diagram

TV02_78

The Kiboriani Mountains are a W-E oriented mountain range making a cut in the general trend of the orogen which is roughly N-S bending around the Tanzania Craton margin (Figs. 1 and 3d). The sample is from a meta-magmatic tonalitic body with the assemblage: Grt-Amph-Bt-Pl-Qtz with the accessoric minerals Ap, Ilm and Zrn. Garnet occurs as poikilitic anhedral crystals which is rich in inclusions of Qtz and Bt and surrounded by fine Bt-laths forming a patchy pattern (Fig. 5a). This type of Grt-Bt intergrowth is typical for the area and already described in more detail by Johnson et al. (2003).

The zircons have an idiomorphic elongated shape and are translucent with tubular inclusions. The internal structures indicate an initial magmatic oscillatory zoning (Fig. 10a). This zoning is partly blurred by subsequent diffusional processes forming lobate structures.

The measured spots are slightly discordant in the diagram (Fig. 10b). With an anchoring spot of 550±50 Ma the upper intercept of the Discordia can be constrained at 2,635±35 Ma.

TV02_51

The Nguru Mountains are also part of the large W-E trending shear system that seems to play a role in the separation of the different tectonic styles in Northern and Central Tanzania (Fig. 1). Those mountains are very remote, hard to reach and display a complicated intercalation of Eastern and Western Granulites. Any geological data are very scarce on this mountain range. The investigated

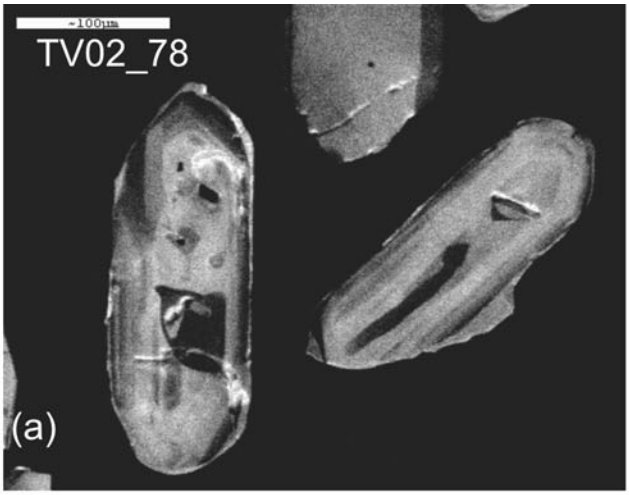
~100µm
TV02_78
(a)

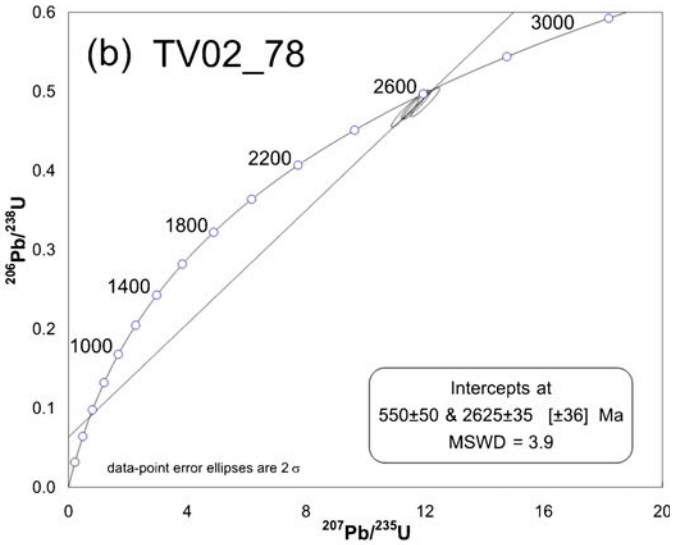
(b) TV02_78
3000
2600
2200
1800
1400
1000
Intercepts at
550±50 & 2625±35 [±36] Ma
MSWD = 3.9
data-point error ellipses are 2 σ
$^{206}Pb/^{238}U$
$^{207}Pb/^{235}U$

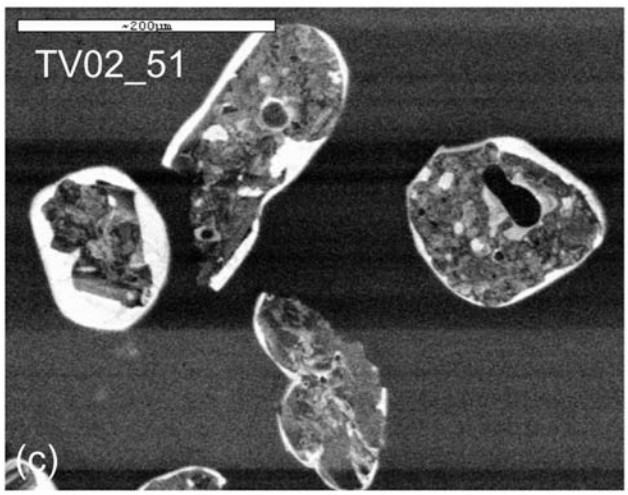
~200µm
TV02_51
(c)

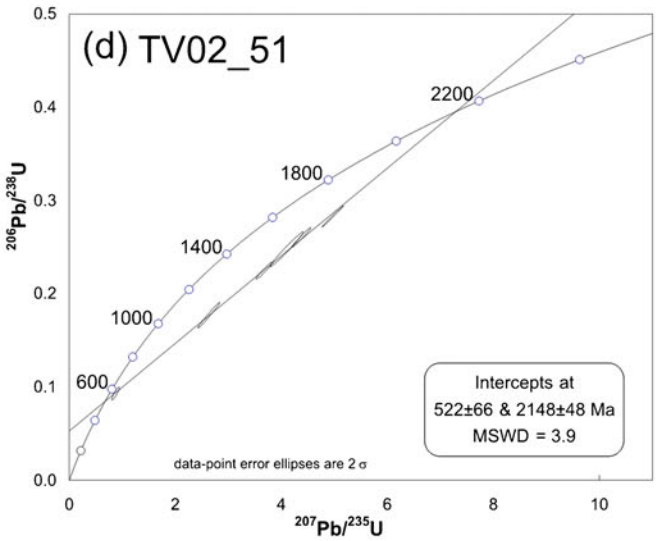
(d) TV02_51
2200
1800
1400
1000
600
Intercepts at
522±66 & 2148±48 Ma
MSWD = 3.9
data-point error ellipses are 2 σ
$^{206}Pb/^{238}U$
$^{207}Pb/^{235}U$

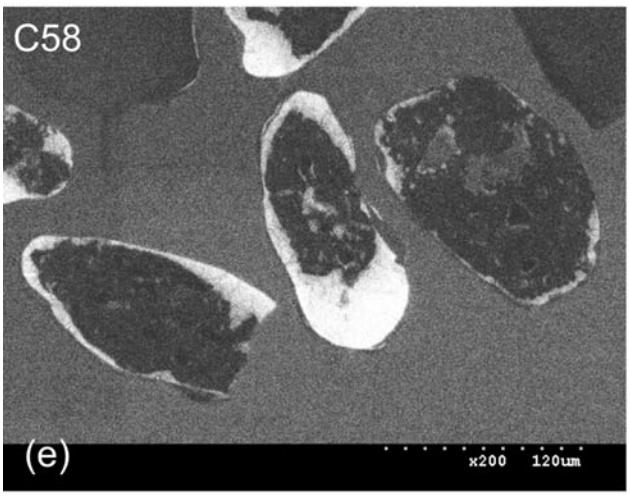
C58
(e)
x200 120um

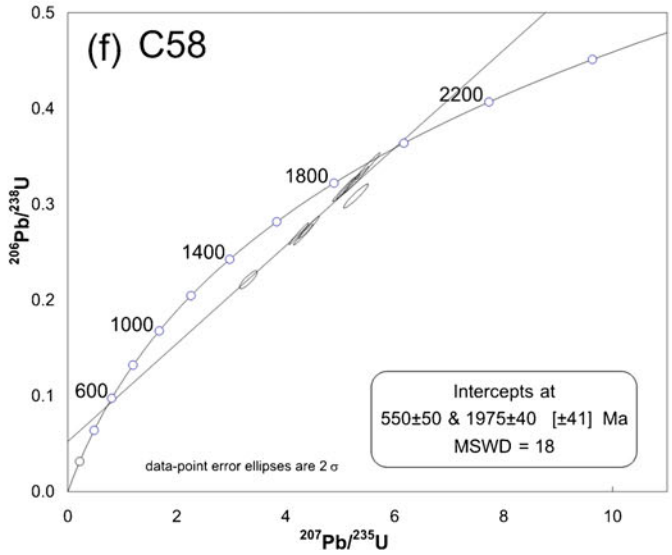
(f) C58
2200
1800
1400
1000
600
Intercepts at
550±50 & 1975±40 [±41] Ma
MSWD = 18
data-point error ellipses are 2 σ
$^{206}Pb/^{238}U$
$^{207}Pb/^{235}U$

sample stems from a tonalitic gneiss exhibiting the mineral assemblage Grt-Hbl-Bt-Ksp-Pl-Qtz (Fig. 5b).

The zircons are irregular rounded grains with opaque red-coloured appearance. The grains resemble partly resorbed cauliflower zircon (Corfu et al. 2003). The internal structure is chaotic-patchy in the core in CL-imaging (Fig. 10c). This pattern is surrounded by a bright overgrowth rim partly diffusing into the patchy core.

Core and rim analyses lie along a discordant line in the diagram (Fig. 10d) and allow the calculation of a lower intercept at 522±66 Ma and an upper intercept age at 2,148±48 Ma.

C58

The southernmost sample of this study is a highly metamorphic amphibolite—a common rock of the Western Granulites (Fig. 1). The mineral assemblage is Grt-Cpx-Bt-Hbl-Pl-Qtz with the typical metamorphic decompression texture of a plagioclase rim around garnet (e.g. Sommer et al. 2008). The garnet is poikilitic with Qtz and Amph inclusions and some Bt-laths. The matrix is mainly composed of Amph with occasional Cpx.

The zircons are elongated to slightly rounded grains with red to brown colour and opaque appearance (Fig. 10e). The CL image shows a patchy dark core with a bright rim forming diffusive irregular lobes into the core. The ages reached through calculation are 1,975±40 Ma for the upper intercept when anchored at 550±50 Ma (Fig. 10f).

## Summary of results

The large meta-magmatic bodies outcropping as inselberg in the Maasai-Steppe (Longido, Lolkisale and Lossogonoi) have Archean crystallization ages with a Kuungan (Cambrian) metamorphic overprint similarly to those from the Craton Boundary (Fig. 11a,b). The degree of metamorphism however is variable. Whereas Lossogonoi did not experience a very high-grade metamorphic overprint in the Neoproterozoic the zircons of Lolkisale show highly diffusive patterns indicating high grade metamorphism. Around Lolkisale the rocks experienced granulite facies metamorphism and the granulites of Loibor Serrit are one of the first Neoproterozoic samples dated in Tanzania by Spooner et al. (1970) with ages around 700 Ma. This indicates that some parts of the Eastern Granulites basement is exposed in vicinity of the Craton margin in the northernmost sections of the Maasai-Steppe. Also the injection of 830 Ma old pegmatites into a basement of unclear origin is new in the study area. The metamorphic age of the pegmatites is 640 Ma, which is a frequent metamorphic age of the Eastern Granulites but in this study area has not been found before. The ages underline a complex intercalation between Western and Eastern Granulite units in a detached basin and dome geometry which has been suggested by Fritz et al. (2009) and LeGoff et al. (2010).

The two ages from the large W-E trending shear systems (Nguru and Kiboriani Shear Belt) display one Archean (2,625 Ma) and one Paleoproterozoic (2,148 Ma) protolith formation age. The distribution of the analysed spots along a Discordia is similar to the majority of the Archean samples from the Craton Boudary with a less-defined lower intercept (here 522 Ma). For comparison a sample typical for the Western Granulites in the southern sequences is added with well-defined ages at 1,975 Ma corresponding to the Usagaran Orogeny. This age indicates that not only Archean basement is reworked in the Western Granulites but also reworked Usagaran Basement can be found at least south of the Kiboriani Shear Belt.

## Interpretation

### *The extent of Usagaran Belt and its tectonic implication*

It can be excluded now, that the magmatic suite of the Usagaran Belt expands from the latitude of Dodoma town further north. North of the Kiboriani Mountains that form a major shear belt (Fritz et al. 2005), no Paleoproterozoic ages typical for the Usagaran Belt are found. Instead, Archean meta-magmatics and meta-sediments were reworked during the late Archean (2.625 Ga) and a late Neoproterozoic (580 Ma) metamorphic event is present in the rocks summarised as the Western Granulites Belt. There are also no relicts of a granulite facies metamorphic event around 640 Ma preserved, that is frequently found in the Eastern Granulites. Instead, there was a metamorphic imprint around 580 Ma (Kuunga Orogeny) as indicated by well-defined monazite ages. These findings are in concordance with Cambrian metamorphic ages derived from Western Granulites crustal xenoliths entrained by young volcanic eruptions next to Arusha (Blondes et al., submitted). Thus, we conclude that the Western Granulites were attached onto the northern Tanzania Craton during the Kuunga Orogeny. In the northernmost part of the Craton Boundary surprisingly Mesoproterozoic magmatic ages around 949±13 Ma appear in the zircons. This age is typically found in the Eastern Granulites in Eastern Tanzania. Hence, we argue that northern portions of Eastern Granulites were thrusted over a large distance closely approaching the Craton margin in the northernmost parts of Tanzania (Fig. 1). The internal deformation and metamorphism of the Eastern Granulites occurred around 620 Ma during the East African Orogeny. During the ca. 550 Ma Kuunga event, the previously assembled Eastern Granulites may have been transported further

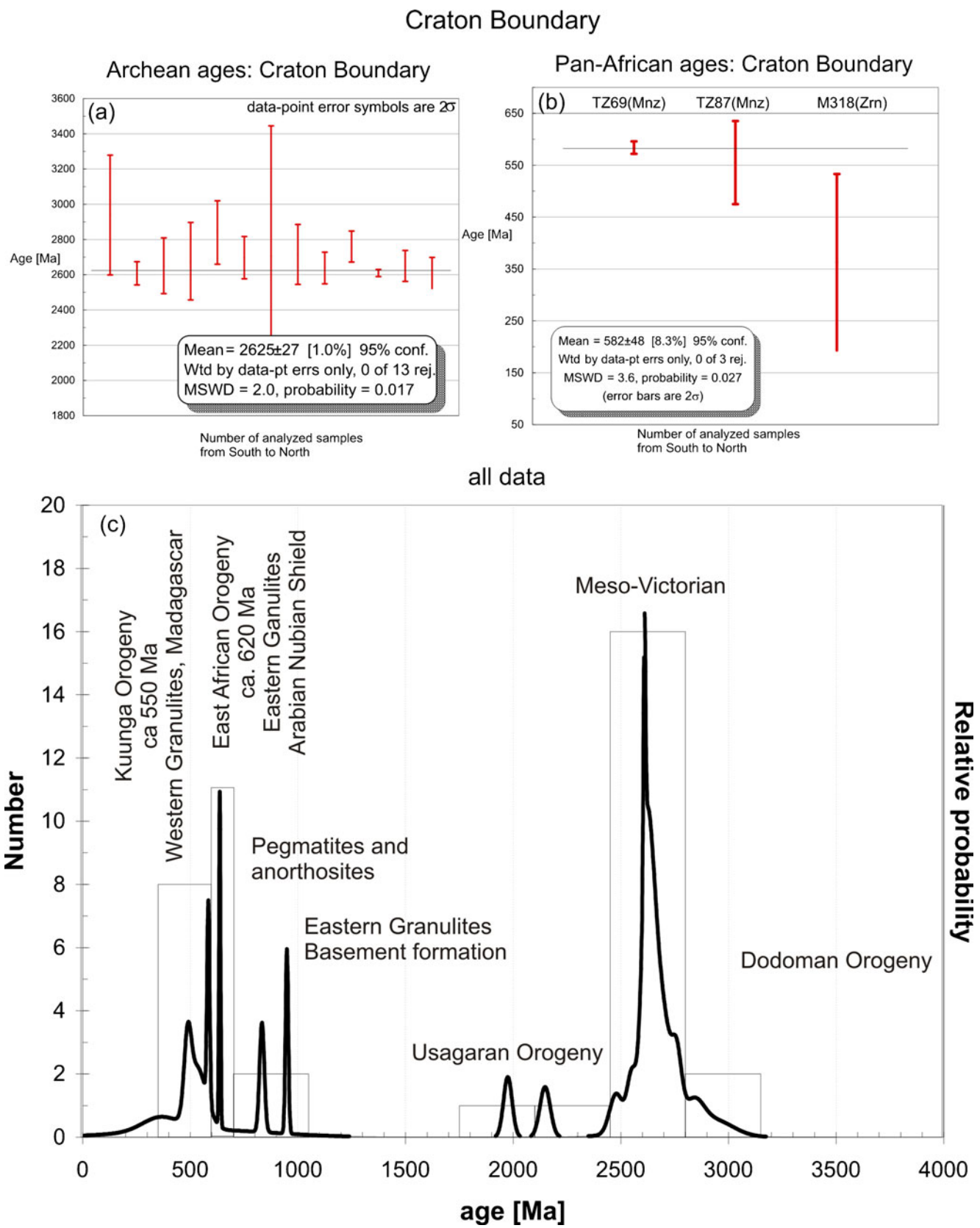


**Fig. 11** Summary diagrams of the collected geochronological data. **a** The Archean ages from zircons of the Craton Margin summarised in a diagram with a weighted mean age added. **b** The monazite ages showing the Kuunga overprint of the Craton Margin summarised in a diagram with a weighted mean age added. **c** Probability density diagram with all data summarised. Tectonic events related to the formation of the Archean Tanzania Craton and the formation of the supercontinent Gondwana are added

westward. Thus, the total nappe emplacement is considered as a sum of two westward directed thrusting events.

*Linking these age provinces into the Rodinia/Gondwana system*

The samples plotted as a probability density plot (Fig. 11c) display a long-lived history within a time array of almost 3 Ga. The peaks represent the times of tectonic events. In the study area a large number of samples plot in the Archean with the highest peak around 2.6 Ga—a phase of intense magmatic activity in the Tanzanian Craton. Pinna et al. (1996) recognised two major periods of crustal growth of the Tanzania Craton. The first event around 2.93–2.85 Ga, the Dodoman Orogeny, is characterised by the formation of typical Archean TTG-suites and granitoids and is localised mainly in the southern part of the Craton around Dodoma. This event was followed by the Victorian Orogeny that summarises a succession of three magmatic/tectonic pulses in the northern part of the Craton and around Lake Victoria. The first phase (Eo-Victorian) shows TTG emplacement (2.73–2.69 Ga), followed by extension-related rhyolite extrusion (2.70 Ga). The second phase (Meso-Victorian) is characterised by bimodal calc-alkaline volcanism (2.66 Ga) with torrential to turbidite sediments intruded by syn-kinematic calc-alkaline granites (2.64 Ga). The third phase (Neo-Victorian) is characterised by syn- to post-collisional granite emplacement (2.60 Ga). The latter are post dated by post orogenic, extension-related rhyolite magmatism at c. 2.53 Ga. Most of our samples stem from the Meso-Victorian magmatic pulse. Similar results have been reached by Mansur et al. (2011) deriving a Meso-Neo-Archean history for the lower crust of the Tanzania Craton and for large parts of the basement of the Mozambique Belt in Northern Tanzania. These authors reported two phases of Archean magmatism around 2.8 and 2.6 Ga and subsequent granulite facies metamorphism in the lower crust.

The Usagaran Orogeny is underrepresented in this diagram. The only true Usagaran finding comes from a sample from the Western Granulites south of the Kiboriani Shear Belt, where reworked Usagaran Basement is widely reported (Sommer et al. 2005). Then, there is a gap of roughly 1 Billion years! The next age domain appears around 1,000 Ma. These ages are typically found in the Eastern Granulites Basement as juvenile crust represented by charnockites and enderbites (Möller et al. 1998).

Subsequent to this period of juvenile crust formation a peak with magmatic ages is seen around 800 Ma (Fig. 11c) as represented by pegmatite formation within the Eastern Granulites. Magmatic ages around 850–880 Ma are typically found within the Arabian Nubian Shield that squeezes out in southern Kenya (Johnson et al. 2011) (Fig. 1). The Arabian Nubian Shield is interpreted to represent the domain where huge masses of Neoproterozoic juvenile oceanic crust have been formed in the course of Rodinia breakup and island arc accretion during the East African Orogeny (ca. 620 Ma). This magmatic event is widely discussed in the literature, and can be related to the formation of vast melt generations during the dispersal of Rodinia (Hoffman 1991; 1999). Meert's (2003) synopsis of the events interpreted the time span between 800 and 700 Ma in Kenya-Tanzania as a time of long-lasting arc magmatism accretion. In Tanzania these ages seem to be restricted to the Eastern Granulites basement (Kröner et al. 2000; Kröner 2001; Tenczer et al. 2006). The Eastern Granulites Belt experienced a coeval magmatism and metamorphism as the Arabian Nubian Shield and hence, is considered as a comparable piece of crust. An obvious difference, however, is the extensive appearance of marbles with depositional ages between 800 and 600 Ma in the Eastern Granulites (Melezhik et al. 2008). We interpret the magmatism in the Eastern Granulites basement as melt generations that intruded into a passive margin on the west-bank of the Mozambique Ocean or alternatively, as magmatic suites intruded during the initial closure of that ocean (Appel et al. 1998). Extensive Andean type arc magmatism at ca. 790 Ma is also reported from Madagascar (Handke et al. 1999; Kröner 2001). The Tanzanian marbles of the Eastern Granulite Belt may have been deposited on the margin of the Mozambique Ocean.

To the East of the Arabian Nubian Shield a piece of Azania, the Galana Terrane is present (Fig. 1). Collins and Pisarevsky (2005) suggested that Azania (Central Madagascar) rifted off East Africa at the time when large volumes of magma formed the Eastern Granulites basement. The Azania margin however was closed around 550 Ma (Kuunga Orogeny), much later than peak metamorphism within the Eastern Granulites and the Arabian Nubian Shield (ca. 620 Ma East African Orogeny). The ca. 550 Ma ages, which are found in the Galana Terrane, are also very frequent in central Madagascar and also in the Western Granulites (Fig. 11). That was the time when different terranes amalgamated at the waning stage of Gondwana collision and the time when the Eastern Granulites achieved their recent position close to the Tanzania Craton margin.

## Conclusions

1) The zircon analyses give ages of several orogenic cycles of the Rodinia-Gondwana system. The majority of data is associated to the crust formation of the Archean Tanzanian Craton (2.5–2.9 Ga) found along the Craton Boundary and in the Western Granulites Belt. Fewer data are found that are representative for the vast volumes of melts generated during the breakup of Rodinia (800–1,000 Ga) as found in the Eastern Granulites Basement. The amalgamation of

various terranes was two-phase. During the East African Orogeny (650–620 Ma) deformation and metamorphism occurred within the Eastern Granulites, approximately coeval with convergence within the Arabian Nubian Shield. The final amalgamation of several terranes forming the supercontinent Gondwana occurred during the Kuunga Orogeny at ca. 550.

2) Two age domains are dominant in the study area of the large and remote Maasai-Steppe in Northern Tanzania. Firstly, an orogenic event of the Tanzanian Craton around 2.6, related to the Meso-Victorian Orogeny and secondly, the ages around 550–580 Ma, the Kuunga Orogeny. The Archean ages are found widespread in the study area either along the Craton Boundary or as reworked basement gneisses in the Western Granulites. They occur also in the cores of large-scale antiforms within the Eastern Granulites and are interpreted as tectonic windows exposing rocks of the Western Granulites.
3) There is no evidence for a northward continuation of the Paleoproterozoic Usagaran Belt that is immediately juxtaposed to the Tanzania Craton south of the study area. This is a result of enhanced shortening and larger thrust emplacement in northern Tanzania when compared to the south. Thrusting was poly-phase; firstly Eastern Granulites were assembled during the East African orogeny. Finally, around 550 Ma further shortening and westward thrusting emplaced Western Granulites onto the Tanzania Craton and Eastern Granulites reached their final position close to the Craton margin. In the course of this event, the Paleoproterozoic Usagaran belt was completely overthrusted.

**Acknowledgements** This paper was financially supported by the Austrian Science Foundation (FWF) Project Nr. T247-N10 and the Swedish Museum of Natural History (HIGHLAT) within the IHP Programme (HPRI-CT-2001-00125) funding the geochronological campaign using the SIMS. For analytical and methodical support at the SIMS M. Whitehouse is thanked. For analytical and support and data reduction using LA-ICP-MS J. Kosler is thanked.

## Appendix

### Analytical procedure for geochronology

The first step in zircon/monazite separation was crushing and sieving to obtain mineral fractions between 63 and 180 μm. Further separation of the heavy minerals was performed with the heavy liquid Na-Polytungstate (SOMETU) and the magnetic heavy minerals were removed by the FRANTZ magnetic separator. Handpicking of the grains was done under the binocular. The mounts were put into epoxy resin together with reference zircon crystal, dried and polished to get a section through the grains centre. For information about the growth structure of the zircons CL and BSE images were taken at the JEOL 6310 SEM in Graz at conditions of 5 nA and 15 kV. One measuring campaign was performed at the Center for Earth Sciences, University of Vienna. There, Zircon/Monazite $^{206}Pb/^{238}U$ and $^{207}Pb/^{206}Pb$ ages were determined with a multi-collector LA-ICP-MS (Nu Instruments HR) coupled to a 193 nm solid state Nd-YAG laser (NewWave UP193-SS) at the Center for Earth Sciences, University of Vienna. Zircons were ablated in a Helium atmosphere, either spot- or raster-wise, and the zonation was derived from CL imaging of each grain. The diameter of spot analyses was 20–50 μm, whereas when scanning, the line widths were 10–35 μm with a rastering speed of 5 μm/s. Energy densities were 5–8 J/cm$^2$ with a laser repetition rate of 10 Hz. The carrier gas (Helium) was mixed with the Argon carrier gas flow prior to the plasma torch. Ablation duration was 60 to 120 s with a 30 s gas- and Hg-blank count rate measurement before ablation started. Ablation count rates were corrected accordingly offline; remaining counts on mass $^{204}$ were interpreted to be common $^{204}Pb$. Static mass spectrometer analysis was as follows: $^{238}U$ was analysed with a Faraday detector, $^{207}Pb$, $^{206}Pb$, and $^{204}$(Pb+Hg) were analysed with ion counter detectors. $^{208}Pb$ was not detected and $^{235}U$ was calculated by the assumption that the ratio $^{238}U/^{235}U$ is 137.88 (Steiger and Jäger 1977). An integration time of 0.2 s was used for all measurements. The ion counter (Faraday and inter-ion counter) gain factors were determined before the analytical session using standard zircon 91500 (Wiedenbeck et al., 1995). Sensitivity on standard zircon 91500 was 30000 cps per ppm for $^{206}Pb$ and 35000 cps for $^{238}U$, respectively. Mass and elemental bias and mass spectrometer drift of both U/Pb and Pb/Pb ratios, respectively, were corrected using a multi-step approach: first-order mass bias is corrected using a dried $^{233}U$-$^{205}Tl$-$^{203}Tl$ spike solution which is aspirated continuously in Ar and mixed to the He carrier gas coming from the laser before entering the plasma. This corrects for bias effects stemming from the mass spectrometer. The strongly time-dependent elemental fractionation coming from the ablation process itself is then corrected for using the "intercept method" of Sylvester and Ghaderi (1997). The calculated $^{206}Pb/^{238}U$ and $^{207}Pb/^{206}Pb$ intercept values are corrected for mass discrimination from analyses of standard 91500 measured during the analytical session using a standard bracketing method. The correction utilises regression of standard measurements by a quadratic function.

A second campaign was performed using a CAMECA IMS1270 ion microprobe at the Swedish Museum of Natural History, Stockholm. Analyses and data reduction procedures follow those outlined by Whitehouse et al. (1997) and references therein. In brief, a ca. 5 nA O2- primary beam was used in aperture illumination mode to sample nominal c. 25 μm elliptical areas. The mass spectrometer was operated in

monocollector mode at a mass resolution of c. 5000, with secondary ions detected using an ion counting electron multiplier. Pb/U ratios, calibrated to 91500 include an error component propagated from the standard analyses in a particular session while Pb-isotope ratio errors are counting statistic based or observed errors. Correction for common lead uses measured $^{204}$Pb and assumes a present day composition from the Stacey and Kramers (1975) model. In many of the samples analysed with very low Pb concentrations, $^{204}$Pb count rates were statistically indistinguishable from background and, in these cases, we have not made a correction. All data reduction was carried out using the routines of Isoplot (Ludwig, 2001).

## References


Appel P, Möller A, Schenk V (1998) High-pressure granulite facies metamorphism in the Pan-African belt of eastern Tanzania: P-T-t evidence against granulite formation by continent collision. J Metamorph Geol 16:491–509

Bellucci JJ, McDonough WF, Rudnick RL (2011) Thermal history and origin of the Tanzanian Craton from Pb isotope thermochronology of feldspars from lower crustal xenoliths. Earth Planet Sci Lett 301:493–501

Blondes MS, Rudnick RL, Ramezani J, Bowring SA, Piccoli PM (submitted) Thermal evolution of the deepest reaches of a continental collision: evidence from U-Pb dating of accessory phases from deep crustal xenoliths from the Pan-African Mozambique Belt, Northern Tanzania. submitted to Contribution Mineralogy and Petrology

Collins AS, Pisarevsky SA (2005) Amalgamating eastern Gondana: the evolution of the zircum Indian Orogens. Earth Sci Rev 71:229–270

Collins AS, Reddy SM, Buchan C, Mruma A (2004) Temporal constraints on Palaeoproterozoic eclogite formation and exhumation (Usagaran Orogen Tanzania). Earth Planet Sci Lett 224:175–192

Corfu F, Hanchar JM, Hoskin PWO, Kinny P (2003) Atlas of Zircon textures. Reviews in Mineralogy and Geochemistry 53:469–500

Cutten H, Johnson SP, deWaele B (2006) Protolith ages and timing of metasomatism related to the formation of whithschists at Mautia Hill, Tanzania: implications for the assembly of Gondwana. J Geol 114:683–698

Feneyrol J, Monié P, Guiliani G, Ohnenstetter D, Malisa E (2011) Panafrican 39Ar/40Ar ages (520–505 Ma) of the tsavorite deposits in the Lelatema Fold Belt (northeastern Tanzania). Geophys Res Abstr 13. EGU2011-3434

Frisch W, Pohl W (1986) Petrochemistry of some mafic and ultramafic rocks from the Mozambique Belt, SE-Kenya.- Mitteilung Österreichischer Geologischer Gesellschaft 78:97–114

Fritz H, Tenczer V, Hauzenberger CA, Wallbrecher E, Hoinkes G, Muhongo S, Mogessie A (2005) Central Tanzanian Tectonic Map (CTTM): a step forward to decipher Pre Pan-African and Pan-African structural events. Tectonics 24:TC6013

Fritz H, Tenczer V, Hauzenberger CA, Wallbrecher E, Muhongo S (2009) Hot granulite nappes—tectonic styles and thermal evolution of the granulite belts in East Africa. Tectonophysics 477:160–173

Gabert G, Wendt I (1974) Datierung von granitischen Gesteinen im Dodoman- und Usagaran- System und in der Ndembera-Serie (Tanzania). Geologisches Jahrbuch, Reihe B 11:3–55

Handke M, Tucker RD, Ashwal LD (1999) Neoproterozoic continental arc magmatism in west-central Madagascar. Geol 27:351–354

Hauzenberger CA, Bauernhofer AH, Hoinkes G, Wallbrecher E, Mathu EM (2004) Pan-African high pressure granulites from SE-Kenya: petrological and geothermobarometric evidence for a polycyclic evolution in the Mozambique belt. J Afr Earth Sci 40:245–268

Hauzenberger CA, Sommer S, Fritz H, Bauernhofer A, Kröner A, Hoinkes G, Wallbrecher E, Thöni M (2007) SHRIMP U–Pb zircon and Sm–Nd garnet ages from granulite facies basement of SE-Kenya: evidence for Neoproterozoic polycyclic assembly of the Mozambique belt. J Geol Soc Lond 164:189–201. doi:10.1144/0016-76492005-081

Hauzenberger CA, Tenczer V, Fritz H, Thöni M (2011) Central Tanzanian granulites from Makubike: a PT-t study.- 23rd Colloquium of African Geology (CAG23), University of Johannesburg, Republic of South Africa, abstract volume, p 184

Hepworth JV (1972) The Mozambique Orogenic Belt and its foreland in northeast Tanzania, a photogeologically-based study. J Geol Soc Lond 128:461–500

Hoffman PF (1991) Did the breakout of Laurentia turn Gondwana inside out? Science 252:1409–1412

Hoffman PF (1999) The break-up of Rodinia birth of Gondwana true polar wander and the snowball Earth. J Afr Earth Sci 28:17–33

Johnson SP, Cutten HNC, Muhongo S, De Waele B (2003) Neoarchaean magmatism and metamorphism of the western granulites in the central domain of the Mozambique belt, Tanzania: U–Pb shrimp geochronology and PT estimates. Tectonophysics 375:125–145

Johnson PR, Andresen A, Collins AS, Fowler AR, Fritz H, Ghebreab W, Kusky T, Stern RJ (2011) Late Cryogenian-Ediacaran 1 history of the Arabian-Nubian Shield: a review of depositional, plutonic, structural, and tectonic events in the closing stages of the northern East African Orogen. Journal of African Earth Sciences, in press.

Kretz R (1983) Symbols for rockforming minerals. Am Min 68:277–279

Kröner A (2001) The Mozambique belt of East Africa and Madagascar: significance of zircon and Nd model ages for Rodinia and Gondwana supercontinent formation and dispersal. S Afr J Geol 104:151–166

Kröner A, Hegner E, Collins AS, Windley BF, Brewer TS, Razakamanana T, Pidgeon RT (2000) Age and magmatic history of the Antananarivo Block central Madagascar as derived from zircon geochronology and Nd isotopic systematics. Am J Sci 300:251–288

LeGoff E, Dechamps Y, Guerrot C (2010) Tectonic implications of new zircon Pb-Pb evaporation data in the Lossogonoi and Longido ruby-districts, Mozambican metamorphic Belt in north-eastern Tanzania. C R Geosci 342:36–45

Ludwig KY (2001) Isoplot/Ex, rev. 2.49. A Geochro No Logical Toolkit for Microsoft Excel. Berkeley Geochronology Center, Special Publication No. 1a

Maboko MAH (1995) Neodymium isotopic constraints on the protolith ages of rocks involved in Pan-African tectonism in the Mozambique Belt of Tanzania. J Geol Soc Lond 152:911–916

Maboko MAH, Boelrijk NAIM, Priem HNA, Verdurmen EATH (1985) Zircon U-Pb and biotite Rb-Sr dating of the Wami River Granulites Eastern Granulites Tanzania: Evidence for approximately 715 Ma old granulite-facies metamorphism and final Pan-African cooling approximately 475 Ma ago. Precambrian Res 30:361–378

Maboko MAH, McDougall I, Zeitler PK (1989) Dating late Pan-African cooling in the Uluguru granulite complex of Eastern Tanzania using the $^{40}$Ar-$^{39}$Ar technique. J Afr Earth Sci 9:159–167

Maboko MAH (2000) Nd and Sr isotopic investigation of the Archean-Proterozoic boundary in north eastern Tanzania: constraints on the nature of Neoproterozoic tectonism in the Mozambique Belt. Precambrian Res 102:87–98

Maboko MAH (2001) Dating post-metamorphic cooling of the Eastern Granulites in the Mozambique Belt of northern Tanzania using the garnet Sm-Nd method. Gondwana Res 4:326–329

Maboko MAH, Nakamura E (2002) Isotopic dating of Neoproterozoic crustal growth in the Usambara Mountains of Northeastern Tanzania: evidence for coeval crust formation in the Mozambique Belt and the Arabian-Nubian Shield. Precambrian Res 113:227–242

Malisa E (1987) Geology of the tanzanite gemstone deposits in the Lelatema area NE Tanzania. Ann Acad Sci Fenn, series A: 146

Mansur AT, Manya S, Timpa S, Rudnick TL (2011) Origin of Archean lower continental crust, Northern Tanzania: a xenolith study. submitted to J Petr

Meert JG (2003) A synopsis of events related to the assembly of eastern Gondwana. Tectonophysics 362:1–40

Melezhik VA, Bingen B, Fallick AE, Gorokhov IM, Kuznetsov AB, Sandstad JS, Solli A, Bjerkgard T, Henderson I, Boyd R, Jamal D, Moniz A (2008) Isotope chemostratigraphy of marbles in north-eastern Mozambique: apparent depositional ages and tectonostratigraphic implications. Precambrian Res 162:540–558

Möller A, Appel P, Mezger K, Schenk V (1995) Evidence for a 2 Ga subduction zone: eclogites in the Usagarian belt of Tanzania. Geology 23:1067–1070

Möller A, Mezger K, Schenk V (1998) Crustal age domains and the evolution of the continental crust in the Mozambique Belt of Tanzania: combined Sm-Nd Rb-Sr and Pb-Pb isotopic evidence. J Pet 39:749–783

Möller A, Mezger K, Schenk V (2000) U-Pb dating of metamorphic minerals: Pan-African metamorphism and prolonged slow cooling of high pressure granulites in Tanzania East Africa. Precambrian Res 104:123–147

Mruma AH (1989) Stratigraphy, metamorphism and tectonic evolution of the early Proterozoic Usagaran Belt, Tanzania. Research Terrae, (Series A), p 193

Mruma AH (1995) Stratigraphy and paleodepositional environment of the Paleoproterozoic volcano-sedimentary Konse Group in Tanzania. J Afr Earth Sci 21:281–290

Muhongo S, Tuisku P, Mtoni Y (1999) Pan-African pressure-temperature evolution in the Merelani area in the Mozambique Belt in North-East Tanzania. J Afr Earth Sci 29:353–365

Pinna P, Cocherie A, Thieblemont D, Feybesse JL, Lagny P (1996) Evolution géodynamique du Craton Est-Africain et déterminisme gitologique. Chronique de Recherche Minie`re 525:33–43

Reddy SM, Collins AS, Mruma A (2003) Complex high-strain deformation in the Usagaran Orogen, Tanzania: structural setting of Palaeoproterozoic eclogites. Tectonophysics 375:101–123

Reddy SM, Collins AS, Buchan AC, Mruma AH (2004) Heterogeneous excess argon and Neoproterozoic heating in the Usagaran Orogen, Tanzania, revealed by single grain 40Ar/39Ar thermochronology. J Afr Earth Sci 39:165–176

Rossetti F, Cozzupoli D, Phillips D (2008) Compressional reworking of the East African Orogen in the Uluguru Mountains of eastern Tanzania at c. 550 Ma: implications for the final assembly of Gondwana. Terra Nova 20:59–67

Sommer H, Kröner A, Hauzenberger CA, Muhongo S, Wingate MTD (2003) Metamorphic petrology and zircon geochronology of high-grade rocks from the central Mozambique Belt of Tanzania; crustal recycling of Archean and Palaeoproterozoic materials during the Pan-African Orogeny. J Met Geol 21:915–934

Sommer H, Kröner A, Muhongo S, Hauzenberger C (2005) SHRIMP zircon ages for post-Usagaran granitoid and rhyolitic rocks from the Palaeoproterozoic terrain of southwestern Tanzania. S Afr J Geol 108:247–256

Sommer H, Hauzenberger Ch, Kröner A, Muhongo S (2008) Isothermal decompression history in the "Western Granulite" terrain, central Tanzania. Evidence from reaction textures and trapped fluids in metapelites. J Afr Earth Sci 51:123–144

Spooner CM, Hepworth JV, Fairbairn HW (1970) Whole rock Rb-Sr isotope investigation of some East African Granulites. Geol Mag 107:511–521

Stacey JS, Kramers JD (1975) Approximation of terrestrial lead isotope evolution by a two-stage model. Earth Planet Sci Lett 26:207–221

Steiger RH, Jäger B (1977) Subcommission on geochronology: convention on the use of decay constants in geo-and cosmochronology. EPSL 36:359–362

Stern RJ (2002) Crustal evolution in the East African Orogen: a neodymium isotopic perspective. J Afr Earth Sci 34:109–117

Sylvester PJ, Ghaderi M (1997) Trace element analysis of scheelite by excimer laser ablation-inductively coupled plasma-mass spectrometry (ELA-ICP-MS using a synthetic silicate glass standard. Chem Geol 141:49–65

Tenczer V, Hauzenberger CA, Fritz H, Whitehouse MJ, Mogessie A, Wallbrecher E, Muhongo S, Hoinkes G (2006) Anorthosites in the Eastern Granulites of Tanzania. New SIMS zircon U-Pb age data, petrography and geochemistry. Precambrian Res 148:85–114

Tenczer V, Fritz H, Bauernhofer A, Hauzenberger CA (2007) Two orogens—one shear belt: 1 Ga of repeated deformation along the Central Tanzanian Shear Belt. J Struct Geol 29:1632–1649

Tenczer V, Hauzenberger CA, Fritz H, Hoinkes G, Muhongo S, Klötzli U (2011) The P–T–$X_{(fluid)}$ evolution of meta-anorthosites in the Eastern Granulites, Tanzania. J Metamorph Geol 29:537–560

Vogt M, Kröner A, Poller U, Sommer H, Muhongo M, Wingate MTD (2006) Archaean and Palaeoproterozoic gneisses reworked during a Neoproterozoic (Pan-African) high-grade event in the Mozambique Belt of East Africa: structural relationships and zircon ages from the Kidatu area, central Tanzania. J Afr Earth Sci 45:139–155

Wiedenbeck M, Alle P, Corfu F, Griffin WL, Meier M, Oberli F, von Quadt A, Roddick JC, Spiegel W (1995) Three natural zircon standards for U-TH-PB, LU-HF, trace element and REE analyses. Geostand Newslett 19:1–23

Whitehouse MJ, Claesson S, Sunde T, Vestin J (1997) Ion microprobe U-Pb zircon geochronology and correlation of Archaean gneisses from the Lewisian Complex of Gruinard Bay northwestern Scotland. Geochim Cosmochim Acta 61:4429–4438